2018

Techno-Economic Analysis of PV Inverter Based Controllers on Low Voltage Distribution Networks

Rupak Mahat
South Dakota State University

TECHNO-ECONOMIC ANALYSIS OF PV INVERTER BASED CONTROLLERS ON LOW VOLTAGE DISTRIBUTION NETWORKS

BY

RUPAK MAHAT

A thesis submitted in partial fulfillment of the requirements for the

Master of Science

Major in Electrical Engineering

South Dakota State University

2018

TECHNO-ECONOMIC ANALYSIS OF PV INVERTER BASED CONTROLLERS ON LOW VOLTAGE DISTRIBUTION NETWORKS

RUPAK MAHAT

This thesis is approved as a creditable and independent investigation by a candidate for the Master of Science in Electrical Engineering degree and is acceptable for meeting the thesis requirements for this degree. Acceptance of this thesis does not imply that the conclusions reached by the candidates are necessarily the conclusions of the major department.

Timothy M. Hansen, Ph.D.
Thesis Advisor Date

Robert Fourney, Ph.D.
Thesis Advisor Date

George Hamer, Ph.D.
Head, Electrical Engineering and Computer Science Date

Dean, Graduate School Date

ACKNOWLEDGEMENTS

I would like to express my sincere gratitude towards my thesis advisors Dr. Timothy M. Hansen and Dr. Robert Fourney for their continuous guidance and encouragement. I would like to acknowledge them for providing valuable insight in every step of this work. This work would not be possible without their patience, motivation, and enthusiasm.

Besides my advisors, I would also like to acknowledge Dr. Reinaldo Tonkoski for his fruitful suggestions on my research. I would also like to thank my graduate faculty representative Dr. Amber Letcher for participation and interest in my work.

I am very thankful to Ujjwol, Manisha, Shaili, Venkat, Fernando for sharing their work and experience with me. I would also like to acknowledge Kapil for helping me organize and review my work. I am grateful to my friends Prateek, Priti, Jyotshana, Anuj for support and encouragement.

Finally, I would like to express my gratitude to my parents, Ram Kumar Mahat and Indira Mahat, my brother Rupesh Mahat for providing me with unfailing support and continuous encouragement throughout my study and research.

CONTENTS

ABBREVIATIONS vii

LIST OF FIGURES viii

ABSTRACT xi

CHAPTER 1 INTRODUCTION 1

1.1 Background 1

1.2 Motivation 3

1.3 Objectives 4

1.4 Contributions 4

1.5 Thesis outline 5

CHAPTER 2 PV INVERTER BASED OVERVOLTAGE CONTROLLER 6

2.1 IEEE standard inverter overvoltage prevention method 6

2.1.1 Active Power Curtailment 7

2.1.1.1 Linear droop-based APC 7

2.1.1.2 Quadratic droop-based APC 8

2.1.2 Combined active and reactive power management 8

2.1.2.1 Normal operating condition 10

2.1.2.2 Linear volt var 10

2.1.2.3 Coordinated reactive power absorption 11

2.1.2.4 Coordinated active power curtailment 12

2.1.2.5 Restoring active power 13

2.1.2.6 Restoring reactive power 14

2.2 Methodology 14

2.3 Co-simulation framework 15

2.4 Benchmark 15

2.5 Implementation of APC in QSTS simulators 16

2.6 Testing and Validating the linear-droop based inverter controller 22

CHAPTER 3 YEAR-LONG SIMULATION OF DIFFERENT TYPES OF PV INVERTER CONTROLLER AND RESULT ANALYSIS 25

3.1 Simulation setup for year-long 25

3.1.1 Controller parameters 25

3.1.2 Load Data 26

3.1.3 PV Data 27

3.1.4 Tariff schemes for customers 27

3.1.4.1 Real-time price 28

3.1.4.2 Fixed rate tariff 29

3.2 Result and analysis 29

3.2.1 Voltage profile 30

3.2.2 Energy generation and loss 33

3.2.3 Impact on distribution transformer loading 40

3.2.4 Financial impact on utility, government, and customers 42

CHAPTER 4 DEVELOPMENT OF 216 HOUSE LARGE DISTRIBUTION FEEDER IN GRIDLAB-D 51

4.1 Benchmark 51

4.2 Feeder validation in PSCAD and GridLAB-D 53

CHAPTER 5 CONCLUSIONS 56

5.1 Conclusions 56

Appendices 57

Appendix CHAPTER A Electrical distribution network parameter for 12 house system 57

Appendix CHAPTER B Electric bill 57

Appendix CHAPTER C Sensitivity 59

Appendix CHAPTER D Electrical distribution network parameter for 216 house system 61

REFERENCES 62

ABBREVIATIONS

APC	Active power curtailment
ARPM	Active and reactive power management
ASC	Aluminum stranded conductors
CAPC	Coordinated active power curtailment
CRPA	Coordinated reactive power absorption
DG	Distributed generation
EMT	Electromagnetic transient
ISO	Independent system operator
LDAPC	Linear droop-based active power curtailment
LVV	Linear volt var
NOC	Normal operating condition
OVP	Overvoltage prevention
PNNL	Pacific northwest national laboratory
PV	Photovoltaic
QDAPC	Quadratic droop-based active power curtailment
QSTS	Quasi-steady-state time-series
RAP	Restoring active power
RPS	Renewable portfolio standard
RRP	Restoring reactive power
RTO	Regional transmission organization
RTP	Real-time pricing

LIST OF FIGURES

Figure 2.1. State transition diagram of the control scheme for the active and reactive power management controller, based on [16]. The value of γ equals 1 if the terminal voltage at any of the inverters exceeds the threshold voltage (V_{th}), else γ equals 0. Time t_{CRPA}, t_{CAPC}, t_{RAP}, and t_{RRP} represent the time at which controller transitions to mode CRPA, CAPC, RAP, and RRP, respectively. 9

Figure 2.2. Bus.py interface for communicating between the PV controllers implemented in Python and GridLAB-D. 16

Figure 2.3. 12 house benchmark feeder with 8.4 kW grid-connected PV installed at each house. 17

Figure 2.4. Numerical oscillation in the voltage at the point of connection of each house of the 12 house test system is shown with a PV power injected changed from 0 kW to 6.25 kW. Similar changes occur with the droop-based APC controllers, due to the large changes in $V - V_{cri}$ or $(V - V_{cri})^2$ in one Δt 17

Figure 2.5. In the event of PV power changing from 0 kW to 6.25 kW, the LDAPC decrease the PV power injection. By making use of the Algorithm 1 the APC is be computed. 22

Figure 2.6. Voltage profile at the point of connection of each house 23

Figure 2.7. Active power exported to the grid after APC is implemented. 24

Figure 3.1. Distribution of voltage magnitudes with and without PV inverter controllers for the year 2014 (6,307,200 voltage magnitude samples from all 12 houses using one-minute time resolution over one year). 31

Figure 3.2. Distribution of voltage magnitudes at different threshold voltages in case of ARPM controller for June 22, 2014. 32

Figure 3.3. Housewise energy generation from PV for year 2014. 34

Figure 3.4. Controller-wise total energy generation for year 2014. 35

Figure 3.5. House-wise net annual energy consumption. 36

Figure 3.6. Controller-wise total energy consumption. 37

Figure 3.7. Annual energy loss due to curtailment and distribution system feeder loss for different types of PV inverter controller. 38

Figure 3.8. Distribution system feeder loss in transformer and distribution line for different types of PV inverter controller. 39

Figure 3.9. Kernel density function for active power, reactive power and apparent power loading of 75 kVA transformer for 2014. 42

Figure 3.10. Annual electric utility charge for each house with different types of PV inverter controller for RTP. 44

Figure 3.11. Annual electric utility charge for each house with different types of PV inverter controller for flat rate tariff. 45

Figure 3.12. Right Y-axis: Comparision of RTP and flat rate tariff prices for a day of June 22, 2014. Left Y-axis: Net transformer power profile with different types of PV inverter controller for a day of June 22, 2014. . . 46

Figure 3.13. Comparision of electric utility bill for RTP and flat rate tariff for different types of PV inverter controller. 47

Figure 3.14. Payback period for 8.4 kW PV system for different PV inverter controller. 48

Figure 3.15. Utility benefit (electric sales minus energy purchase from ISO) with and without considering distribution system losses (higher is better for ComEd). The top-right box gives the cost of distribution system losses for the different types of PV inverter controllers. 49

Figure 3.16. Taxes and fees charges for different PV inverter controller for RTP and flat rate tariff. 50

Figure 4.1. 216 house benchmark system under consideration. 52

Figure 4.2. Voltage profile in low voltage side (a) simulated in GridLAB-D (b) simulated in PSCAD. 54

Figure 4.3. Voltage profile in medium voltage side (a) simulated in GridLAB-D (b) simulated in PSCAD. 54

Figure 4.4. Voltage error between GridLAB-D and PSCAD (a) low voltage side (b) medium voltage side. 55

ABSTRACT

TECHNO-ECONOMIC ANALYSIS OF PV INVERTER BASED CONTROLLERS ON LOW VOLTAGE DISTRIBUTION NETWORKS

RUPAK MAHAT

2018

Voltage-rise due to increasing installation of photovoltaic (PV) systems is a major technical issue in low voltage distribution networks. A cost-effective approach to address the overvoltage problem is to control the active and reactive power provided by the existing PV inverters. Prior research used electro-magnetic transient (EMT) simulation tools to develop inverter control strategies for overvoltage prevention. These type of simulation requires high computational resources and simulation time, and is therefore not suitable for long time period studies (e.g., annual) with many inverters. With the anticipated high penetration of PV, there is a desire for a suitable tool for long time-horizon simulation studies to perform technical and economic analysis. This research work describes the use of quasi-steady-state time-series (QSTS) software (GridLAB-D) to implement inverter overvoltage prevention strategies (formerly developed using EMT simulation), allowing previously infeasible long-term techno-economic analysis of such controllers. A co-simulation framework is used to coordinate the PV inverter controllers implemented in Python on a 12-house low voltage distribution network model developed in GridLAB-D. Three PV inverter controllers are implemented to evaluate the long term technical and economic aspects, including voltage profile analysis, energy generation and consumption, system losses, and transformer

loading. Two different pricing structures, real-time pricing (RTP) and flat rate tariff, have been considered in the economic analysis. It is shown that with high penetration of PV and use of effective inverter controllers, the financial benefit to the end-users increases significantly when a net metering policy is used to trade electricity in either tariff scheme. This, however, caused a reduction in the utility electricity sales, and governmental taxes, possibly leading to increased electric rates over time. In addition a 216 house 3 phase distribution feeder is developed in GridLAB-D which can further be used for evaluating different PV inverter controller for large test case system.

CHAPTER 1 INTRODUCTION

1.1 Background

The installation of photovoltaic (PV) generation in residential systems is increasing rapidly due to increasing environmental concerns, decreasing costs of PV modules, and governmental incentives [1]. Distributed PV systems are connected to low/medium voltage distribution systems in the form of distributed generation (DG), but increased PV installation has led to operational problems [2]. Distribution systems need to operate within parameters related to voltage regulation, power quality, system protection, reliability, and others. The operating conditions of such systems is not acceptable if specified conditions are violated.

One of the important limiting factors that determine the operation of DG is the voltage regulation. The national standard for voltage regulation in the United States is set by the ANSI voltage regulation standard C84.1 [3], which states that under normal operating conditions voltage levels should not exceed 1.042 per-unit (p.u.). The amount of power generated by distributed PV with a distribution circuit can be increased until a violation of the extreme operating condition of 1.058 p.u. defined by ANSI standard. Once the threshold is reached no more PV generation can be incorporated. Traditionally, utilities use voltage compensation techniques based on line voltage drop from the substation considering unidirectional power flow to the end user. However, with the increasing installation of PV, power flow is not always unidirectional, which can lead to voltage-rise in distribution feeders [4]. Several case studies in real distribution system show the problem of voltage-rise due to increased penetration of PV power generation. An

electric distribution system in Germany with 160 inverters totaling 440 kW solar capacity exceeded overvoltage limit set by European standard [5]. Similarly, in a distribution system with 553 residential PV customers (2.1MW capacity in total) in Ota, Japan, showed a voltage rise up to 0.027 p.u. during peak PV generation [6]. In [7], a simulation study conducted on Porterville feeder of California showed up to 11% rise in voltage for 300% penetration level (defined as ratio of PV rating to annual peak load).

Different approaches to solve the voltage-rise problem due to high PV penetration in distribution systems have been discussed in the literature. Traditional voltage regulating devices, such as line voltage regulators [8], switched capacitor banks [9], and on-load tap changing transformers are some of the conventional approaches to prevent overvoltage in distribution systems, but they cannot act in a sufficiently short time interval and thus result in poor regulation [10]. Additionally, even if these approaches were to limit the voltage fluctuations, the high number of switching operations would shorten their operational life. As an alternative, utilities can increase the conductor size (decrease conductor resistance) of distribution lines to prevent voltage-rise. However, reconstruction of the distribution system is expensive, complicated, and time-consuming [11].

PV inverter control methods for preventing overvoltage in low voltage distribution feeders are widely studied in literature. Popular approaches in network independent PV inverter overvoltage control are active power curtailment (APC) based on voltage deviations [12], [13], reactive power absorption based on linear Volt/Var droop [14], [15], and active and reactive power management using limited communication [16]. However, long-term technical and economic impact studies of such inverter controllers are still missing from literature. One reason for this is the use electromagnetic transient (EMT)

simulators to test the inverter controllers for preventing overvoltage, such as in [12], [13], [16], which is computationally burdensome. An alternative to EMT simulation is to use quasi-steady-state time-series (QSTS) simulation, which uses the converged steady-state solution of the current time-step as the initial state of the next iteration to solve sequential steady-state power flow equations [17]. These simulation tools require less computational resources (i.e., faster) than EMT simulation to calculate system state, as QSTS does not consider power system dynamics. In [14], the Volt/Var PV control method was tested using a QSTS method, but the impact on feeder loss and transformer loading caused by increased reactive power flow through the distribution feeder was not considered, nor the economic analysis of such controllers.

1.2 Motivation

Increasing PV generation in low voltage distribution system increases income for those electric customers with PV by selling the energy. This generation of energy at the distribution level reduces cost of transmission and generation of bulk power, thus saving large amount of investment. More PV in the distribution system results in reverse power flow and creates an increase in voltage. It is necessary to maintain distribution voltage at the limit for safe operation of electric appliances. Currently a PV inverter turn off approach which is simple and robust method is used to maintain the voltage. Turning off the PV inverter causes large energy curtailment and reduces the revenue. An overvoltage control method that maintains the voltage within the maximum limit while reducing overall energy loss is desirable.

1.3 Objectives

The main objective of the research work is to analyze different types of PV inverter overvoltage controller based on the yearly simulation on voltage limiting capability, energy generation, loss in the distribution system, curtailment energy loss. In addition, performing the economic analysis of two different tariff rates for PV owned house, and finding its impact for the government, utility, and customer point of view are other objectives.

1.4 Contributions

The primary contributions of this thesis are:

(a) a 12 house radial distribution system based on [12] is developed in GridLAB-D, a QSTS distribution system simulator, to perform long-term technical and economic analysis,

(b) technical performance of different PV inverter controllers specifically three in this research work: inverter overvoltage prevention, active power curtailment, and active and reactive power management are evaluated by considering their impact on overvoltage prevention, energy generation, distribution system losses, and transformer loading. Also economic impacts on the utility, government, and end-user are evaluated using net-metering with different pricing structures, specifically real-time pricing (RTP) and flat rate tariff,

(c) a sensitivity-based algorithm to prevent numerical oscillation caused by droop-based PV inverter control methods in QSTS simulators is designed,

(d) a 216 house three phase distribution feeder based on [18] is developed and validated in GridLAB-D which can be further use for evaluating PV inverter controller.

1.5 Thesis outline

This thesis is organized as follows: Chapter 2 describes overview and implementation of PV inverter controller for overvoltage prevention. The year long simulation and the techno-economic analysis is presented in Chapter 3. Chapter 4 describes the development of simulation test bench of a large distribution feeder in GridLAB-D. Concluding remarks are provided in Chapter 5.

CHAPTER 2 PV INVERTER BASED OVERVOLTAGE CONTROLLER

Increasing PV power injection in low voltage distribution systems may cause reverse power flow from end-users to the distribution substation. The rise in local voltage caused by the active and reactive power generation (e.g., from PV or other DG) in a distribution system can be approximated as [12]:

$$\Delta V = \frac{PR + QX}{V} \tag{2.1}$$

where P and Q are the net active and reactive power injected by a house with DG, and R and X are the resistance and reactance of the feeder connecting the house to the substation, respectively. For a given distribution system, overvoltage caused by increasing the amount of installed DG (PV in this case) can be prevented by curtailing active power and/or absorbing reactive power. The active and reactive power is controlled by the PV inverter, which has already been installed in the system to convert DC power from PV to AC power, resulting in a low-cost method for overvoltage prevention.

2.1 IEEE standard inverter overvoltage prevention method

The simplest approach to control overvoltage is to shut down the inverter when the local voltage exceeds above the defined threshold value. In the IEEE 1547 standard [19], this threshold value is defined as 1.1 p.u., or alternatively this can be set to upper limit of the extreme operating range defined by the ANSI C84.1-1989 standard [3] (which is 1.058 p.u.). In this approach, the PV inverter operates at maximum active power, P_{MPPT}, at a unity power factor until the voltage at the point of connection reaches a maximum

threshold voltage, V_{th}. If the local voltage rises above V_{th}, the inverter output is set to 0. The re-connection time for inverters after shutdown is required to be a minimum of five minutes [19]. In this research work, this method is refered as the inverter overvoltage prevention (OVP) approach. Although simple, the major disadvantage of this approach is the large increase in total energy curtailment, especially with a high-level of installed PV, leading to reduced financial benefits for the owner. A more effective approach would be, partially curtailing the active power from PV inverter based on local voltage measurement as explained in the next section.

2.1.1 Active Power Curtailment

In active power curtailment (APC) approach, the PV inverter curtails its active power output as a function of the deviation of the local voltage from a critical voltage. The critical voltage is typically defined as a value near the overvoltage limit. There are different methods for implementing APC; in this research work, we implemented the common linear droop-based approach from [12], and the quadratic droop-based appproach from [13] for comparison purpose.

2.1.1.1 Linear droop-based APC

The most common method for implementing APC is using a linear gain proportional to the deviation of the voltage from a critical voltage value, V_{cri}. In this method, denoted linear droop-based APC (LDAPC), the PV active power output, P_{inv}, is given by [12]:

$$P_{inv} = \begin{cases} P_{MPPT} - m(V - V_{cri}), & \text{if } V \geq V_{cri} \\ P_{MPPT}, & \text{if } V < V_{cri} \end{cases} \tag{2.2}$$

where P_{MPPT} is the maximum power available in the PV array for a given solar irradiance (kW), m is a linear droop coefficient (kW/V), and V is the local grid voltage at the PV inverter (V). From (2.2), the LDAPC controller curtails $m(V - V_{cri})$ active power (kW) when $V \geq V_{cri}$ (i.e., the voltage rises above the critical threshold).

2.1.1.2 Quadratic droop-based APC

Another approach for APC was proposed in [13], using a *quadratic* droop as opposed to the linear droop from the LDAPC controller in the previous section. In this quadratic droop based APC (QDAPC), the amount of APC is determined by a quadratic function, where the curtailment is proportional to the *square* of the deviation of the voltage from V_{cri}. By using the quadratic droop, the amount of power curtailed is lower for small voltage deviations, resulting in less energy curtailment through time. The PV active power output of the QDAPC controller is given by:

$$P_{inv} = \begin{cases} P_{MPPT} - q(V - V_{cri})^2, & \text{if } V \geq V_{cri} \\ P_{MPPT}, & \text{if } V < V_{cri} \end{cases} \tag{2.3}$$

where q is the quadratic droop coefficient (kW/V^2). The QDAPC controller curtails $q(V - V_{cri})^2$ active power (kW) when $V \geq V_{cri}$.

2.1.2 Combined active and reactive power management

Although reactive power has less of an impact on voltage compared to active power (because $R >> X$ in (2.1) in low-voltage distribution lines), it can reduce the active power curtailment required to prevent overvoltage. By reducing the curtailment of active power, the end user receives increased financial benefits. Additionally, reactive power does not

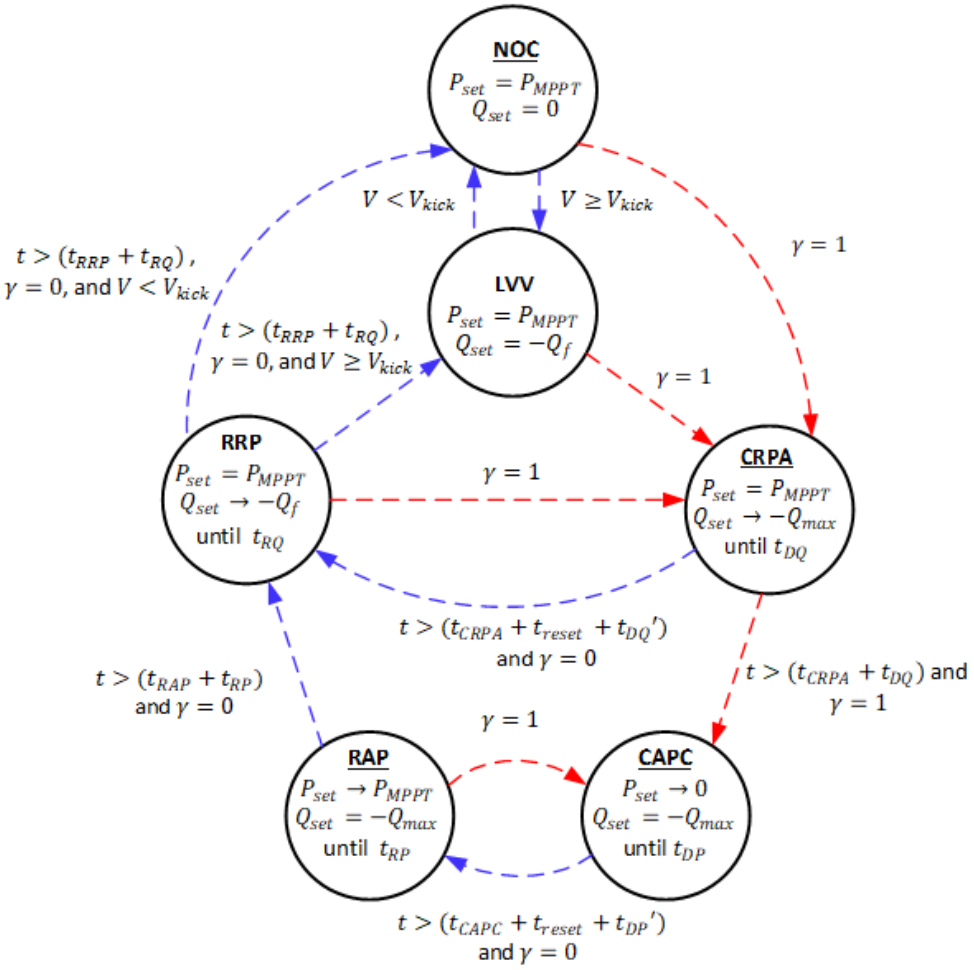

Figure 2.1. State transition diagram of the control scheme for the active and reactive power management controller, based on [16]. The value of γ equals 1 if the terminal voltage at any of the inverters exceeds the threshold voltage (V_{th}), else γ equals 0. Time t_{CRPA}, t_{CAPC}, t_{RAP}, and t_{RRP} represent the time at which controller transitions to mode CRPA, CAPC, RAP, and RRP, respectively.

directly contribute to a monetary benefit or loss, although the utility may see an increase in feeder and transformer losses.

The combined active and reactive power management (ARPM) controller uses the latent reactive power capacity of the inverters to attempt to correct overvoltage before starting to curtail active power. In this controller from [16], a global communication

signal, γ, is used to effectively coordinate distributed inverters to control active and reactive power set-points for preventing overvoltage. Assuming the inverter is designed for a minimum power factor of ϕ_{min}, the maximum reactive power an inverter can utilize at time t, $Q_{max}[t]$, is dependent on the current active power set-point, $P_{set}[t]$, by:

$$Q_{max}[t] = P_{set}[t]\tan(\cos^{-1}(\phi_{min})) \tag{2.4}$$

The state diagram representing the correlation between different modes of operation is presented in Fig. 2.1. The different modes are discussed in detail below.

2.1.2.1 Normal operating condition

The ARPM will be in the normal operating condition (NOC) mode when no PV terminal voltages in the distribution feeder exceed the kickoff voltage (V_{kick}). In this mode, the global communication signal is not issued by any house (i.e., $\gamma = 0$), the active power of each inverter is set to P_{MPPT}, and the reactive power is set to 0. If at any house, the local voltage, V, exceeds V_{kick}, but is less than V_{th}, the associated inverter will move to the linear volt var (LVV) mode (i.e., $V_{kick} \leq V < V_{th}$, $\gamma = 0$). It is possible that $V \geq V_{th}$ at a house in the distribution feeder while other inverters are in mode NOC. In such a case, the inverter with $V \geq V_{th}$ will issue a global signal (i.e., $\gamma = 1$), and all inverter controllers transition to the coordinated reactive power absorption (CRPA) mode.

2.1.2.2 Linear volt var

In LVV, the controller operates by adjusting the reactive power of the PV inverter as a function of local voltage V, given by (2.5), while the active power remains at P_{MPPT}.

$$Q_f = \frac{-Q_{max}}{V_{th} - V_{kick}} \times (V - V_{kick}) \tag{2.5}$$

Every inverter absorbs reactive power independently ($\gamma = 0$). Absorbing reactive power locally helps to not only reduce the chances of overvoltage occurring, but also avoids the need of substantial reactive power absorption from coordinated reactive power management. To achieve this objective, a kick off voltage, $V_{kick}(< V_{th})$, is defined after which all inverters will start absorbing reactive power in linear fashion corresponding to the local voltage.

If $V \geq V_{th}$ at any inverter point of connection, the associated inverter will issue the global communication signal, $\gamma = 1$, and all inverter controllers will transition to the coordinated reactive power absorption (CRPA) mode.

2.1.2.3 Coordinated reactive power absorption

If absorbing reactive power locally in mode LVV does not solve the overvoltage problem, the excess reactive power capacity of the other inverters that are not experiencing overvoltage can be used to attempt to bring the voltage below the threshold value. Let t_{CRPA} be the time the controllers transition to CRPA, and t_{DQ} be the maximum time the controllers will stay in mode CRPA. In CRPA, every inverter will start to increase reactive power absorption towards Q_{max} at time $t = t_{CRPA} + t_{DQ}$, while the active power remains at P_{MPPT}. If Δt is the simulation timestep, the reactive power setpoint for each inverter at time t is computed by:

$$Q_{set}[t] = Q_{set}[t-1] + (-Q_{max}[t] - Q_{set}[t-1])\frac{\Delta t}{t_{CRPA} + t_{DQ} - t} \tag{2.6}$$

CRPA can transition to two different modes, depending on whether overvoltage persists after $t = t_{CRPA} + t_{DQ}$. If overvoltage persists, all inverters will transition to the coordinated active power curtailment (CAPC) mode. Otherwise, they will transition to the restoring reactive power (RRP) mode after $t = t_{CRPA} + t'_{DQ} + t_{reset}$. Here, t'_{DQ} is the actual time controllers are in CRPA mode with $\gamma = 1$ ($t_{DQ'} \leq t_{DQ}$). The reset time, t_{reset}, is required to prevent sudden voltage changes which may occur if the reactive power is immediately restored.

2.1.2.4 Coordinated active power curtailment

If the overvoltage problem is not resolved even when all inverters absorb their maximum reactive power, the active power injected by each inverter must be curtailed to prevent overvoltage. This is performed collaboratively in CAPC mode. In CAPC, the reactive power of each inverter remains at Q_{max}, while the active power is curtailed towards zero from t_{CAPC} to $t_{CAPC} + t_{DP}$, where t_{CAPC} is the time the controllers transitioned to CAPC, and t_{DP} is time it takes the controllers to reach an active power output of 0. The active power set-point, P_{set}, at time t is given by:

$$P_{set}[t] = \begin{cases} P_{set}[t_{CAPC}]\left(1 - \frac{\Delta t}{t_{CAPC} + t_{DP} - t}\right), t < t_{CAPC} + t_{DP} \\ 0,\ t \geq t_{CAPC} + t_{DP} \end{cases} \tag{2.7}$$

If the overvoltage is mitigated at all inverter locations before $t = t_{CAPC} + t_{DP}$, each PV controller keeps its active power setpoint constant until $t = t_{CAPC} + t'_{DP} + t_{reset}$, when they will transition to restoring active power (RAP) mode and γ is set to 0. Here, t'_{DP} is the actual time controllers are in CAPC mode with $\gamma = 1$. Again, t_{reset} is the time required to prevent sudden voltage changes that may occur due to immediate active power restoration.

2.1.2.5 Restoring active power

The purpose of RAP mode is to restore the active power injection of all inverters once the overvoltage problem is resolved. In RAP mode, each inverter controller locally restores active power towards P_{MPPT} within t_{RRP} to $t_{RRP} + t_{RP}$, where t_{RRP} is the time the controllers transitioned to RAP, and t_{RP} is the maximum amount of time the controllers will stay in mode RAP. The reactive power of each inverter remains at Q_{max}, and the active power setpoint for each inverter is given by:

$$P_{set}[t] = P_{set}[t-1] + (P_{MPPT}[t] - P_{set}[t-1]) \frac{\Delta t}{t_{RRP} + t_{RP} - t} \tag{2.8}$$

If overvoltage occurs at any inverter during active power restoration ($V \geq V_{th}$), the global signal is issued ($\gamma = 1$) and all inverters transition back to CAPC mode. Otherwise, if $V < V_{th}$ after $t = t_{RRP} + t_{RP}$, the inverter controllers transition to the restoring reactive power (RRP) mode.

2.1.2.6 Restoring reactive power

Once the active power is fully restored and there is no overvoltage at any point in the distribution system, reactive power absorption of each inverter is reduced from Q_{max} to reduce system losses caused by increased reactive power absorption. In RRP, γ remains at 0, active power of each inverter remains at P_{MPPT}, and the reactive power absorption is reduced to match the reactive power corresponding to the local voltage (i.e., from the local droop in LVV mode) within time t_{RRP} to $t_{RRP}+t_{RQ}$, where t_{RRP} is the time the controllers transitioned to RRP, and t_{RQ} is the maximum time the controllers will stay in mode RRP. The reactive power setpoint in this mode is given by:

$$Q_{set}[t] = Q_{set}[t-1] + (Q_f[t] - Q_{set}[t-1])\frac{\Delta t}{t_{RRP}+t_{RQ}-t}. \tag{2.9}$$

If $V \geq V_{th}$ in RRP, the global signal will be issued, and all inverters will transition back to CRPA. Otherwise, if $V < V_{th}$ after $t = t_{RRP}+t_{RQ}$, the controller will transition to either NOC ($V < V_{kick}$) or LVV ($V_{kick} < V < V_{th}$).

2.2 Methodology

This research works compares three different PV inverter controllers described in Section 2.1 based on their long term technical and economic impact in low voltage distribution systems. Although our framework is applicable to any system, for this example the 12 house radial distribution system from [20] implemented in a QSTS simulator is used. Each house is assumed to have a grid-connected PV inverter. In Section 2.3, a co-simulation framework for interfacing different PV controllers to a QSTS

simulator is described. Section 2.4 gives a detailed overview of the low voltage distribution system under consideration. Section 2.5 describes implementation of APC in QSTS simulators.

2.3 Co-simulation framework

To implement the controllers and evaluate their impact on the distribution grid GridLAB-D, a distribution system simulation software is used. GridLAB-D is an open-source QSTS simulation tool developed by the U.S. Department of Energy at the Pacific Northwest National Laboratory (PNNL) [21]. Two options were considered for implementing a controller in GridLAB-D: (i) writing the controller in C++ within GridLAB-D and re-compiling, and (ii) using an external controller with a co-simulation framework to change GridLAB-D parameters based on the control algorithm during runtime. One such co-simulation tool is Bus.py [22], which uses Python to pass messages between one or more instances of GridLAB-D. The PV inverter controllers are implemented in Python. Bus.py is then used to pass the control signals to GridLAB-D, as shown in Fig. 2.2.

2.4 Benchmark

We implemented a benchmark in GridLAB-D to demonstrate the value of the framework in comparing the performance of different overvoltage prevention controllers based on [12]. The benchmark is a typical 12 house radial distribution system, with each house having an installed peak PV capacity of 8.4 kW. The houses are supplied through a 75 kVA, single-phase, 14.4 kV - 120/240 V distribution transformer as shown in Fig. 2.3. The feeder is 120 m long, with two live wires twisted around a grounded neutral cable

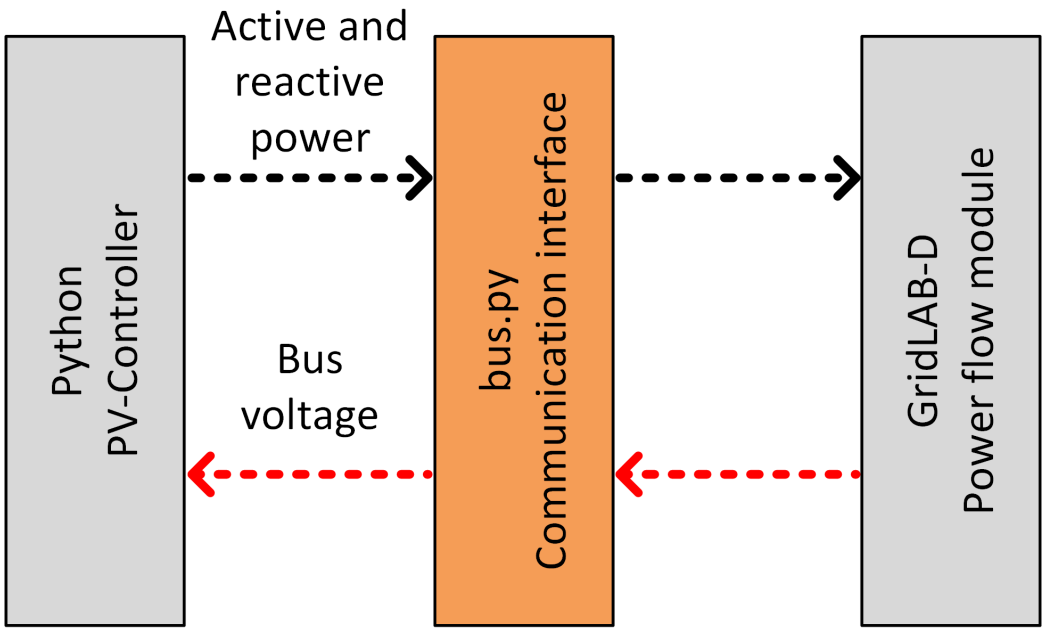

Figure 2.2. Bus.py interface for communicating between the PV controllers implemented in Python and GridLAB-D.

(NS 90 3/0 AWG). The service entrance consists of two wires supported by a steel grounded neutral cable (NS 90 1/0 AWG). Each house in the distribution feeder is 20 m from the main distribution line. The line parameters of the benchmark feeder are provided in Tables A.1 and A.2 in the Appendix A.

2.5 Implementation of APC in QSTS simulators

While implementing droop-based APC in QSTS simulation software, a phenomenon of numerical oscillation is observed. This section describes the cause of the numerical oscillation, and presents a solution. For explanatory purposes, the PV power of each house in the 12 house benchmark is changed from 0 kW to 6.25 kW with the LDAPC controller in Fig. 2.4 and the resulting numerical oscillations caused by the controller

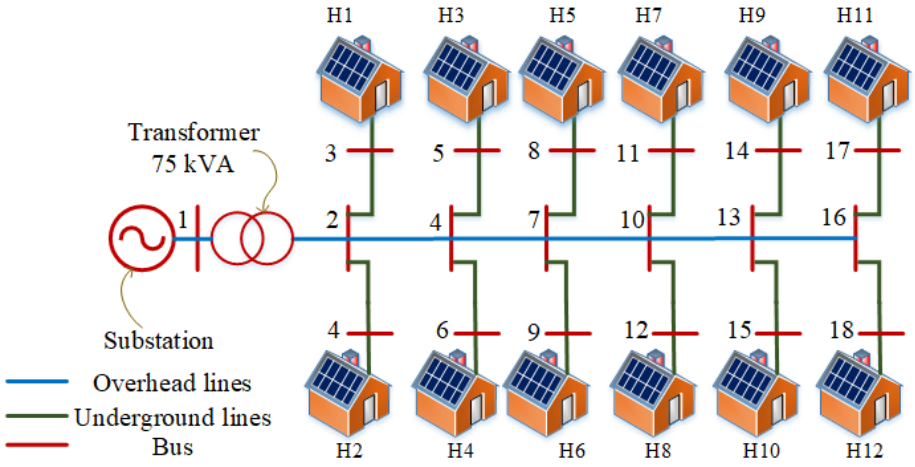

Figure 2.3. 12 house benchmark feeder with 8.4 kW grid-connected PV installed at each house.

response at each house are shown.

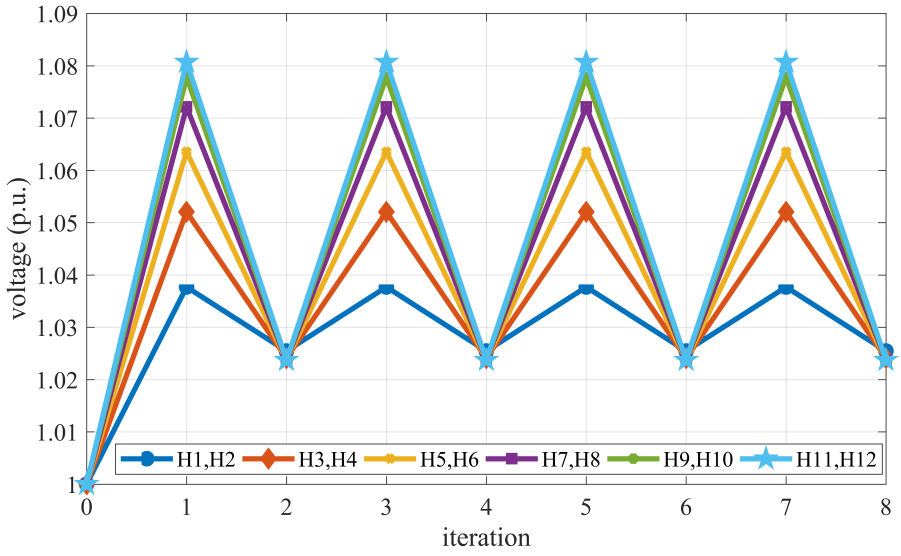

Figure 2.4. Numerical oscillation in the voltage at the point of connection of each house of the 12 house test system is shown with a PV power injected changed from 0 kW to 6.25 kW. Similar changes occur with the droop-based APC controllers, due to the large changes in $V - V_{cri}$ or $(V - V_{cri})^2$ in one Δt

When implementing the system using QSTS simulation software, the system dynamics are neglected having step changes from one time period to the next. The implemented droop controller thus generates control actions based on these steady-state

RMS values at every iteration, causing the numerical oscillations in voltage. When the voltage observed by the controller is high, the curtailment of power from PV is high based on (2.2). This, in turn, leads to a significant drop in voltage. The high level of curtailment then causes the voltage to go below the critical voltage, causing the controller to inject the maximum amount of PV available (P_{MPPT}). This cyclic process continues indefinitely as seen in Fig. 2.4.

For solving the numerical oscillation problem, a technique is proposed to iteratively determine the required APC for each PV inverter at each discrete timestep in the QSTS simulator. The proposed technique is described in Algorithm 1 for the LDAPC controller. At the beginning of a simulation, the simulation parameters (initial voltage, critical voltage, initial APC, and droop coefficient of each inverter) are initialized as shown in initialization block. After initialization, for each timestep of the QSTS simulator, the active power output of each PV inverter is iteratively determined by using a sensitivity matrix based on the distribution network parameters and the distribution system state (e.g., load).

Let V and δ be the voltage magnitude and angle at a distribution bus, respectively, and P and Q be the net injected active and reactive power, respectively. The oscillation issue can be addressed by using a voltage sensitivity index ($\Delta V/\Delta P$) to determine the level of curtailment. This index increases or decreases the curtailment based on a voltage sensitivity index which attempts to estimate the change in voltage due to a level of curtailment of active power. The amount of curtailment is iteratively calculated during subsequent time-steps until the voltage converges to a steady-state value (e.g., in Fig. 2.5). A sensitivity matrix for a power system network ($\mathbf{S_V}$) consists of partial derivatives that

represent the change in voltage magnitude and angle ($\Delta V, \Delta\delta$) of each bus due to the changes in active and reactive power ($\Delta P, \Delta Q$) at each bus.

For an N-bus power system network, the voltage sensitivity matrix in compact notation can be written as,

$$\mathbf{S_V} = \begin{bmatrix} (\frac{\Delta\delta}{\Delta P}) & (\frac{\Delta\delta}{\Delta Q}) \\ (\frac{\Delta V}{\Delta P}) & (\frac{\Delta V}{\Delta Q}) \end{bmatrix}_{2N\times 2N} \tag{2.10}$$

A sensitivity matrix, $\mathbf{A}$, of the change in voltage magnitude with respect to the active power can be defined as a submatrix of the voltage sensitivity matrix.

$$\mathbf{A} = \left[\frac{\Delta V}{\Delta P}\right]_{N\times N} \tag{2.11}$$

Let $\mathcal{N} := \{2, 3, ...N\}$ be a set of buses in a distribution system, not including the slack bus. We define $\mathcal{N}_g \subseteq \mathcal{N}$ as a collection of the buses where DG (in this case where the PV inverters) is connected, and $H = |\mathcal{N}_g|$. Let $\mathbf{S}$ be an $H \times H$ sensitivity matrix with element $\mathbf{S}_{i,j} \in \mathbf{A}$ corresponding to the sensitivity of DG bus i with respect to DG bus j, $\forall\, i, j \in \mathcal{N}_g$.

At iteration n, let $\mathbf{v}^{(n)}$ and $\mathbf{v_{cri}}$ be vectors of size H containing the measured voltage magnitude at each PV inverter and the critical voltage, respectively, and $\mathbf{p_c}^{(n)}$ be a vector of size H of the active power curtailed at each PV inverter. To calculate the curtailed active power at iteration n, we set

$$\mathbf{p_c}^{(n)} = \mathbf{p_c}^{(n-1)} + \Delta\mathbf{p_c}^{(n)}, \tag{2.12}$$

where $\Delta\mathbf{p_c}^{(n)}$ is the change in active power curtailed from iteration $n-1$ to n.

Let $\mathbf{v}^{*(n)}$ be a vector of size H which is *estimated* voltage magnitude at each PV inverter given a curtailed power of $\mathbf{p}_c^{(n)}$, given as:

$$\mathbf{v}^{*(n)} = \mathbf{v}^{(n)} - \mathbf{S}\Delta\mathbf{p_c}^{(n)}. \tag{2.13}$$

Using the LDAPC relation from (2.2), curtailment for estimated voltage $\mathbf{v}^{*(n)}$ can also be calculated as:

$$\mathbf{p_c}^{(n)} = m(\mathbf{v}^{*(n)} - \mathbf{v_{cri}}). \tag{2.14}$$

Merging (2.12) and (2.14), we obtain

$$\mathbf{p_c}^{(n-1)} + \Delta\mathbf{p_c}^{(n)} = m(\mathbf{v}^{*(n)} - \mathbf{v_{cri}}). \tag{2.15}$$

Substituting $\mathbf{v}^{*(n)}$ in (2.15), we get:

$$\mathbf{p}_c^{(n-1)} + \Delta\mathbf{p}_c^{(n)} = m(\mathbf{v}^{(n)} - S\Delta\mathbf{p}_c^{(n)} - \mathbf{v}_{cri}) \tag{2.16}$$

$$\Delta\mathbf{p_c}^{(n)}(m\mathbf{S} + \mathbf{I}) = m(\mathbf{v}^{(n)} - \mathbf{v_{cri}}) - \mathbf{p_c}^{(n-1)} \tag{2.17}$$

$$\Delta\mathbf{p_c}^{(n)}\mathbf{B} = \mathbf{a} \tag{2.18}$$

$$\therefore \Delta\mathbf{p_c}^{(n)} = \mathbf{B}^{-1}\mathbf{a} \tag{2.19}$$

where $\mathbf{a} = m(\mathbf{v}^{(n)} - \mathbf{v_{cri}}) - \mathbf{p_c}^{(n-1)}$, $\mathbf{B} = m\mathbf{S} + \mathbf{I}$, and $\mathbf{I}$ is the identity matrix.

After calculating $\Delta\mathbf{p_c}^{(n)}$, active power curtailment is obtained using (2.12). Let $\mathbf{p_{MPPT}}$ be a vector of size H denoting the maximum active power available at each PV inverter, $\mathbf{p_{inv}}$ be a vector of size H denoting the active power output of each PV inverter, and $\mathbf{c}$ is a binary vector of size H where each element is $\in 0, 1$ based on $\mathbf{v}^{(n)} \geq \mathbf{v_{cri}}$. At each iteration n, the PV inverter power is set to $\mathbf{p_{inv}^{(n)}} = \mathbf{p_{MPPT}} - \mathbf{c} \odot \mathbf{p_c^{(n)}}$ (i.e., $\mathbf{p_{MPPT}}$ if $V < V_{cri}$, otherwise curtailed according to $\mathbf{p_c}^{(n)}$). The algorithm continues until $||\mathbf{v}^{(n)} - \mathbf{v}^{(n-1)}||_\infty \leq \varepsilon$, where $\varepsilon > 0$ is a stopping tolerance.

Algorithm 1: Implementing the LDAPC controller

Input:

- Critical Voltage $\mathbf{v_{cri}}$
- Droop Coefficients m
- Initial Inverter voltage $\mathbf{v}^{(n)}$
- Initial Curtail power $\mathbf{p_c}^{(n)}$

Data:

- Read PV power $\mathbf{p_{MPPT}}$
- Read house load power

while $||\mathbf{v}^{(n)} - \mathbf{v}^{(n-1)}||_\infty > \varepsilon$ **do**
  $\Delta\mathbf{p_c}^{(n)} = \mathbf{B}^{-1}\mathbf{a}$
  $\mathbf{p_c}^{(n)} \leftarrow \mathbf{p_c}^{(n-1)} + \Delta\mathbf{p_c}^{(n)}$
  $\mathbf{p_{inv}^{(n)}} \leftarrow \mathbf{p_{MPPT}} - \mathbf{c} \odot \mathbf{p_c^{(n)}}$
  solve load flow with $\mathbf{p_{inv}}^{(n)}$
  $n \leftarrow n + 1$
end
return $\mathbf{p_{inv}}$

Using Algorithm 1 for a 12 house distribution feeder with the sensitivity matrix set to the value given in [12], the problem of the numerical oscillation has been solved as

shown in Fig. 2.5.

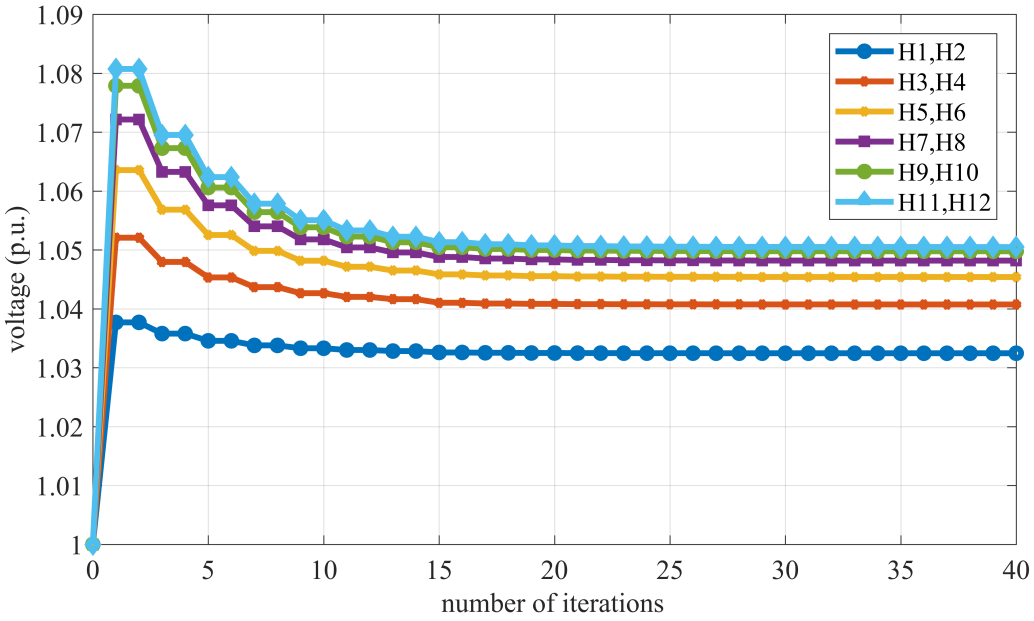

Figure 2.5. In the event of PV power changing from 0 kW to 6.25 kW, the LDAPC decrease the PV power injection. By making use of the Algorithm 1 the APC is be computed.

Similarly, curtailment for QDAPC is calculated using

$$\mathbf{p_c}^{(n)} = q(\mathbf{v}^{*(n)} - \mathbf{v_{cri}})^2. \tag{2.20}$$

Equations (2.12), (2.13), and (2.20) are solved for $\Delta\mathbf{p}_c^{(n)}$. The obtained value of $\Delta\mathbf{p}_c^{(n)}$ is updated in line 3 of Algorithm 1 while implementing QDAPC.

2.6 Testing and Validating the linear-droop based inverter controller

After implementing the corrective solution of the oscillation described in Section 2.5, the voltage profile of 12 houses are obtained by varying net power from -75 kW to 75 kW as shown in Fig. 2.6 where negative power indicate load condition and positive power indicate generation.

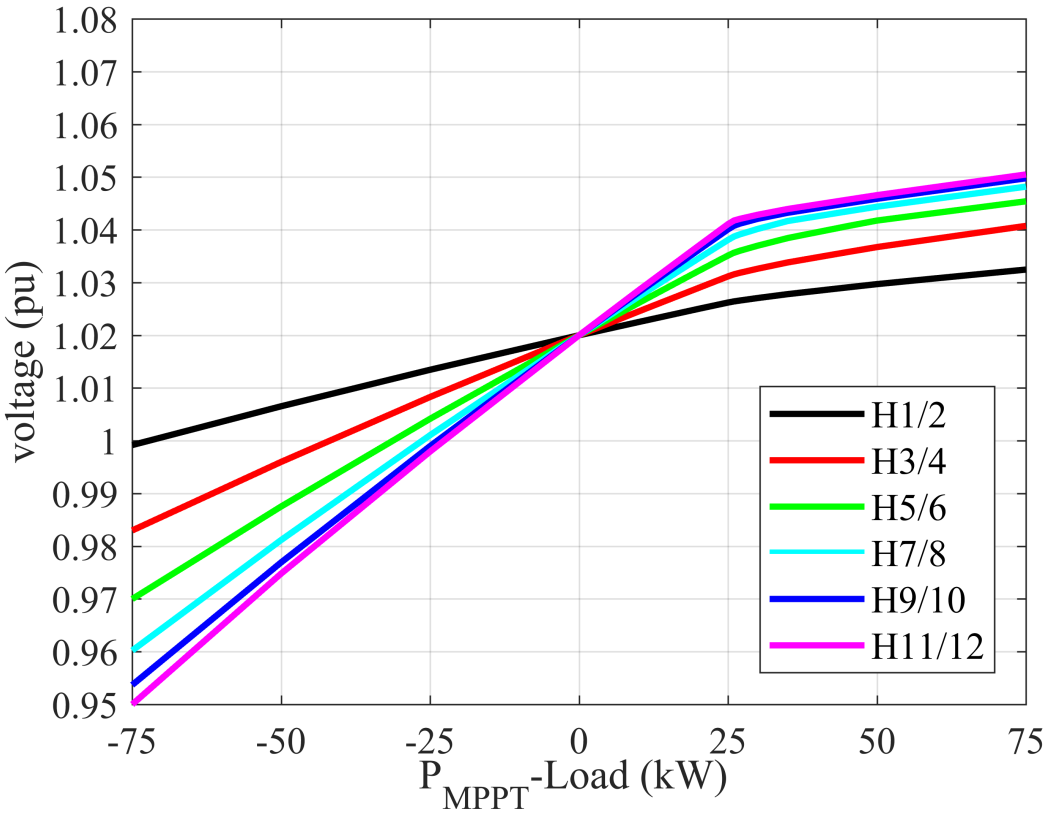

Figure 2.6. Voltage profile at the point of connection of each house

For validation of the proposed algorithm, the voltage for H11/H12 obtained after implementing the algorithm and voltage from paper [20] is shown in Table 2.1 for comparison between between the voltage profile obtained from the developed algorithm and the voltage profile obtained using PSCAD. The results are comparable, with the maximum deviation of voltage from the original paper being just 0.038%. This validates the replication of the controller and test benchmark in the QSTS software GridLAB-D interfaced with Python.

Fig. 2.6 presents the feeder voltage profile at the PCC of each house. The maximum voltage was found to be 1.05049 p.u., which is less than that of voltage without the APC. Fig. 2.7 shows the power injected by each house, where all houses except H1/2, and H3/4

curtail the power during voltage rise is observed.

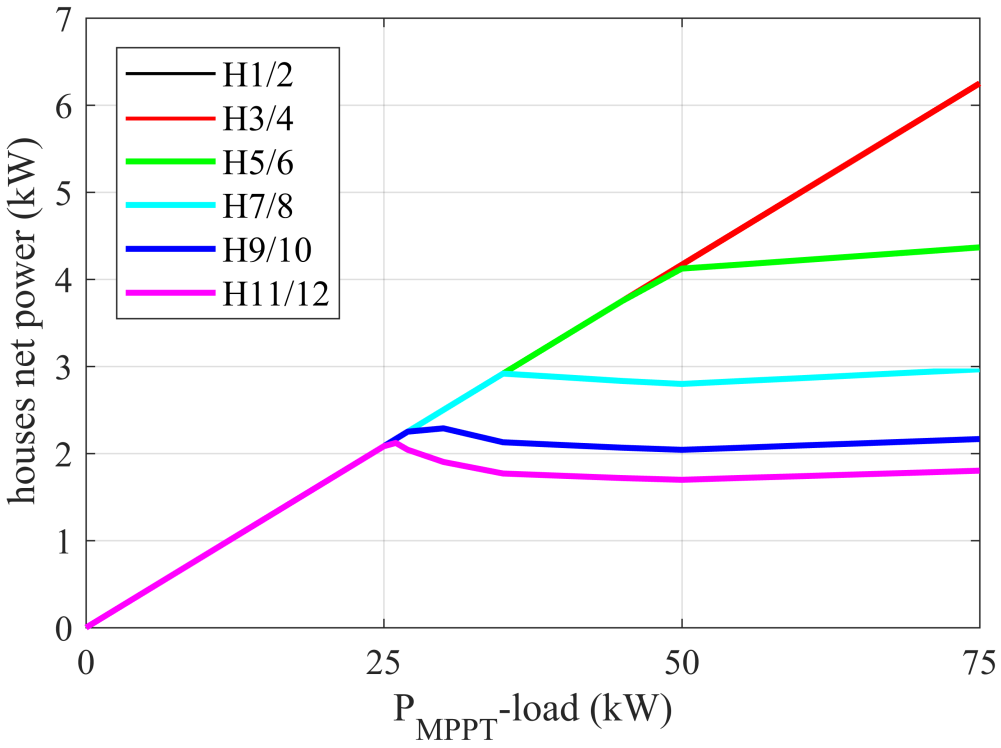

Figure 2.7. Active power exported to the grid after APC is implemented.

Table 2.1. Comparison of voltage at H11/12 house between GridLAB-D and original paper [20].

Total Power (kW)	Voltage (p.u) GridLAB-D	Voltage (p.u.) Paper [20]
25	1.04108	1.04070
27*	1.04207	1.04200
30	1.04285	1.04245
35	1.04394	1.04399
40	1.04482	1.04474
45	1.04570	1.04529
50	1.04656	1.04620
55	1.04735	1.04729
60	1.04813	1.04852
65	1.04892	1.04854
70	1.04970	1.04972
75	1.05049	1.05080
* At 27 kW of net generation, inverter starts to curtail active power		

CHAPTER 3 YEAR-LONG SIMULATION OF DIFFERENT TYPES OF PV INVERTER CONTROLLER AND RESULT ANALYSIS

3.1 Simulation setup for year-long

This section describes the input data for load, irradiance, and electricity pricing, and provides the PV controller parameters used in our simulation study. The methods described above, however, are general enough to be used in any distribution network with any set of inputs and controller parameter settings.[1]

3.1.1 Controller parameters

PV inverter controllers using OVP, LDAPC, QDAPC, and ARPM are implemented in each inverter of a 12 house test benchmark using the specific parameters given in Table 3.1. Threshold and critical voltage values are chosen based on ANSI C84.1 std. [3], specifically V_{th} is set to upper limit of normal operating range and V_{cri} is set to the upper limit of critical operating range. Similarly, V_{kick} is set to the distribution transformer tap setting point (note, this remains constant in our simulation). The droop coefficients for LDAPC and QDAPC are computed such that no curtailment occurs below the voltage V_{cri} and full capacity curtailment occurs when voltage reaches V_{th} and this variation of curtailment is linear in former and quadratic in later controller. The voltage error (ε) in proposed algorithm is chosen as 0.001 V. The time parameters for ARPM controllers are obtained from [16]. The simulation time step is one minute, and the minimum power factor is set 0.95.

[1] Our GridLAB-D models, data, and Python controllers can be found online at https://github.com/rmahat/Distribution-Network-GLM-file

Table 3.1. Simulation Parameters Selected for the Benchmark

Threshold voltage (V_{th})	1.058 p.u.
Critical voltage (V_{cri})	1.042 p.u.
Kickoff voltage (V_{kick})	1.02 p.u.
Linear droop coefficient (m)	2.1 kW/V
Quadratic droop coefficient (n)	0.57 kW/V^2
t_{DQ} , t_{DP} , t_{reset}	10 min
t_{RQ} , t_{RP}	20 min
Δt	1 min
ϕ_{min}	0.95

Note that these values are chosen for this comparative study, but the method is general and can be used for any combination of input parameters.

3.1.2 Load Data

Unique load data was created for each house using the $M_t/G/\infty$ queue model from [23]. This queue model creates unique random loads for each house that statistically approximate an expected home load, $l(t)$, with the aggregate load of all homes matching a known distribution system load profile. The model makes use of the openly available hourly load data from distribution companies to create a time varying arrival rate for the $M_t/G/\infty$ queue model, where the arrival times indicate house loads turning on. For this simulation, load from the ComEd (the utility company for Chicago, IL) area of PJM for the year 2014 was scaled down according to (3.1) to fit each house of the test system [24]. At time t, let $C_L(t)$ be the load of the ComEd area, and b_{min} and b_{max} be scaling factors set to 100 W and 5000 W, respectively. These values were selected to model characteristics of the test system, e.g., transformer rating, PV panel rating.

$$l(t) = b_{min} + \frac{C_L(t) - min(C_L)}{max(C_L) - min(C_L)} \cdot (b_{max} - b_{min}) \tag{3.1}$$

3.1.3 PV Data

Solar radiation data for calculating available PV power is obtained from SolarAnywhere [25], a web-based service that provides hourly irradiance for various locations in the USA. Our study considers Chicago, IL, at a latitude of 41.88° N and a longitude of 87.66° W for the year 2014 to match the synthetic load data. Solar data required for our one minute simulation time-step is calculated from the hourly data using linear interpolation. Irradiance data is then used to calculate the maximum power available in the PV array:

$$P_{MPPT} = \eta \times I \times A. \tag{3.2}$$

Where η is the efficiency of the PV panel, I is solar irradiance in W/m^2, A is the area of PV panel in m^2. For a PV panel of 8.4 kW capacity, the efficiency is taken as 16.7% and an area of 50.2605 m^2 [26].

3.1.4 Tariff schemes for customers

For the electric bill calculation, a sample ComEd electric bills from [27] and [28] are used. In general, the electric bill is divided into three categories: supply charge, delivery charge, and tax & fees. These categories are explained in Section 3.1.4.1. For selling PV energy to the grid, the PV customers are assumed to be in a net metering program in which the customer will sell electricity at the same rate they pay for

consumption. Two types of tariff schemes, real-time pricing (RTP) and a flat-rate tariff are explained in this section. The different supply, delivery, and taxes & fees of the two schemes are shown in Appendix B in Tables B.1, B.2, and B.3, respectively.

3.1.4.1 Real-time price

ComEd RTP can be divided into three parts [28]. First, the supply charge is subdivided into an energy consumption charge, capacity charge, and transmission charge. The energy consumption charge is calculated using the hourly RTP, averaged from 5-minute RTP blocks provided by ComEd [29]. The capacity charge is per kW, computed based on the customer's contribution to ComEd's system peak, multiplied by the monthly peak kW for that house. The transmission charge is designed to allow the utility to recover costs associated with transmission, calculated based on the kWh consumption.

Second, the delivery charge is subdivided into a fixed charge, distribution facility charge, and an Illinois electricity distribution charge. The fixed charge is applied to each consumer for metering and service. The distribution facility charge is the charge to recover costs to install and maintain the electric delivery system, calculated as a per kWh price multiplied by the total energy consumption of the customer over the billing period. The Illinois electricity distribution charge includes incremental Distribution uncollectible cost factor to recover uncollectible cost.

Finally, the taxes & fees category contains state tax, municipal tax, and several named taxes regarding state and federal policy: Environmental Cost Recovery Adjustment, Renewable Portfolio Standard, Zero Emission Standard charge, and Franchise cost. State tax and municipal tax are cents per kilowatt-hour (¢/kWh) charges

applied to the kilowatt-hours (kWhs) delivered to customers [30]. Environmental Cost Recovery Adjustment covers clean-up costs at gas-manufacturing sites. Renewable Portfolio Standard (RPS) is a charge to compensate utility payment for an obligation on electricity supply companies to produce a specified fraction of their electricity from renewable energy sources. Zero Emission Standard charge which is paid as a subsidy for zero-carbon power generators. Franchise cost is a cost utilities impose on their customer for a cost paid to some cities in exchange for the right to deliver electricity to them.

3.1.4.2 Fixed rate tariff

The ComEd fixed rate tariff is similar to RTP tariff, but instead of using a varying hourly rate, energy prices are calculated at a fixed rate (constant throughout the billing period) per kWh of energy [27]. The fixed rate tariff can also be divided into three section of supply, delivery, and taxes & fees. The supply charge is based on only kWh consumption. Delivery charges for fixed rate tariff are similar to RTP. Taxes & Fees charged are also similar to RTP, except an energy efficiency programs charge is included. Under the public utilities act, ComEd recovers the costs of energy efficiency and demand-response programs designed to help consumers save money. This per kWh charge covers programs such as air-conditioner cycling, appliance recycling, and hourly pricing.

3.2 Result and analysis

The performance of the different inverter controllers for overvoltage prevention in LV distribution system caused by the increasing PV injection is analyzed in this research work. Voltage distribution, energy (both generation & loss) , transformer loading and effect of two different types of tariff schemes (flat rate & RTP) are compared step by step.

The performance of the different inverter controllers for overvoltage prevention in LV distribution system caused by increasing levels of PV installation is analyzed in this section using the parameters outlined above. Voltage profile, energy (both generation & loss), transformer loading and effects of two different types of tariff schemes (flat rate & RTP) on end user and utility are compared for inverter controllers discussed above.

3.2.1 Voltage profile

A violin plot showing the distribution of voltage magnitudes for each controller, compared to the baseline case without overvoltage protection control (i.e., maximum power output at all times, regardless of voltage issues), is presented in Fig. 3.1. This type of plot is similar to a box plot, but with the (rotated) kernel density plot on each side. The thickness (or density) represents how often each voltage magnitude occurred. In Fig. 3.1, the shape of the distribution of voltage magnitudes within the range of 1.042 p.u. and 1.058 p.u. for each controller (this is the operating zone for the inverter controllers) reflects the controller response to overvoltage and also provides information about energy being curtailed by its implementation.

The voltage magnitudes are clustered closer to the upper limit (1.058 p.u.) for QDAPC, whereas they are clustered near lower limit (1.042 p.u.) in LDAPC. The ability of the QDAPC controller to maintain the voltage near the maximum limit more often than LDAPC is because the QDAPC controller curtails less active power for voltages near the lower limit (quadratic behavior). Thus, QDAPC greatly reduces total energy curtailment compared to the LDAPC while still maintaining the voltage within the limits. Notice that a cluster near the upper limit, as exhibited by the APC controllers, will reduce the energy

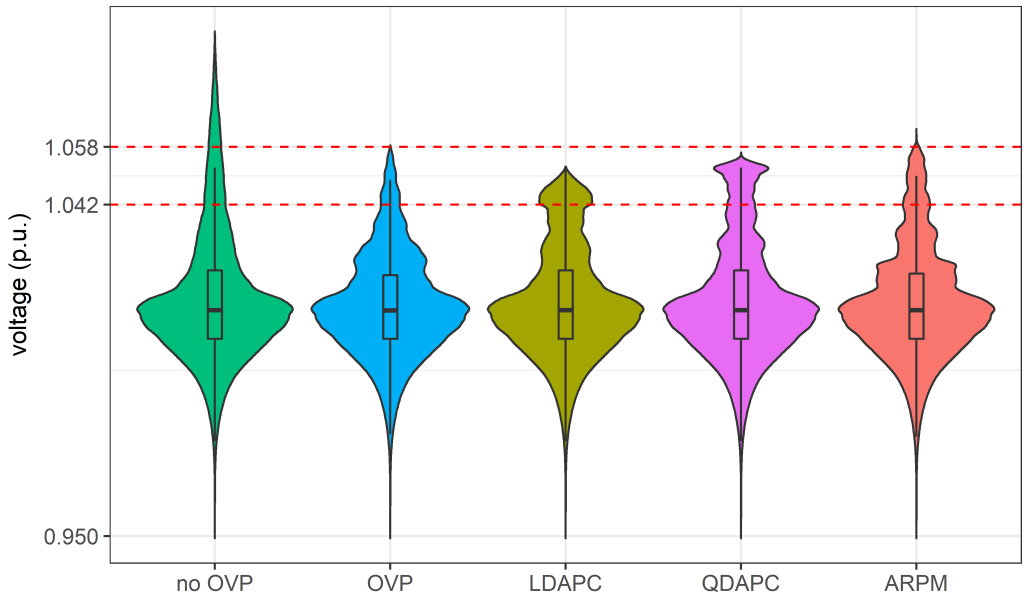

Figure 3.1. Distribution of voltage magnitudes with and without PV inverter controllers for the year 2014 (6,307,200 voltage magnitude samples from all 12 houses using one-minute time resolution over one year).

being curtailed. In case of the OVP inverter controller, because the inverter shuts down (full curtailment) and remains off for five minutes after the occurrence of overvoltage, the voltage drops instantly once curtailment commences. This causes the clustering of voltage magnitudes near 1.058 pu (note, this controller does not make use of the 1.042 p.u limit).

The lower density of voltage magnitudes in the range between 1.042 p.u. and 1.058 p.u. in the ARPM controller compared to LDAPC and QDAPC is because, most of the time in the region of interest, the controller is absorbing reactive power to avoid overvoltage, while injecting maximum available power from the PV. The ARPM will have lowest curtailment, shown in the next section.

If no overvoltage protection is implemented, the system will reach a peak voltage of 1.09 p.u. The minimum voltage in the system is 0.95 p.u. and remains unaffected by the implementation of the inverter controllers (note, the control of undervoltage is not within

the scope of this research work). It is also important to mention that in this simulation study, the voltage at H1 to H4 never exceed the critical voltage, indicating that local inverter control approaches (OVP, LDAPC, and QDAPC) will not curtail active power at these houses to prevent overvoltage like ARPM, as ARPM takes a coordinated approach to control overvoltage. All controllers are able to maintain the voltage below 1.058 p.u. except for the ARPM controller. This is because of the inherent characteristics of ARPM algorithm, in which the communication signal is issued only when the voltage of a house is above 1.058 p.u. and it takes certain time for other houses to ramp their reactive power absorption to the maximum limit.

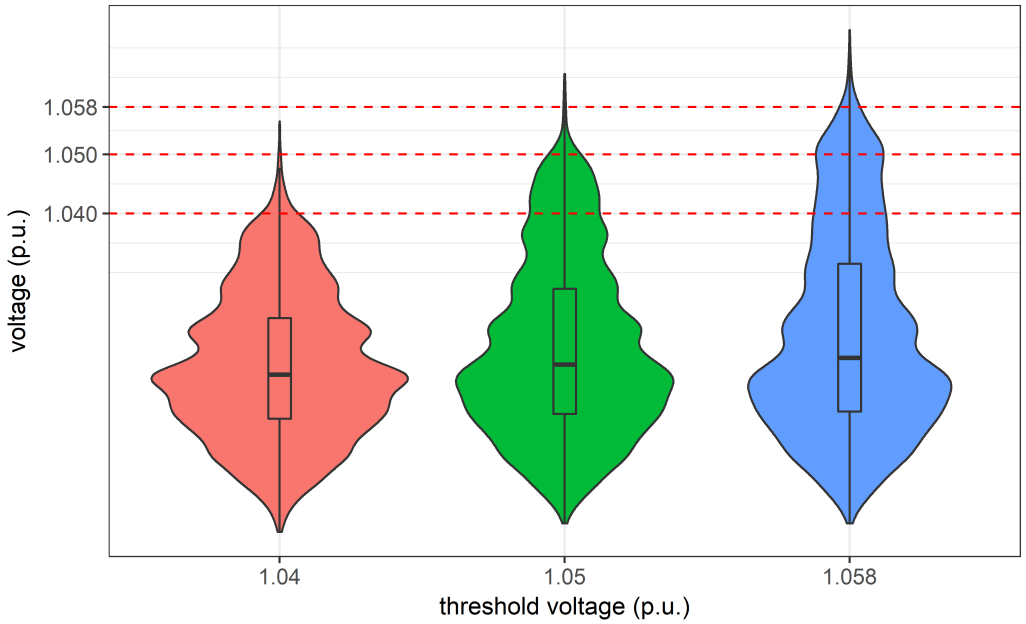

Figure 3.2. Distribution of voltage magnitudes at different threshold voltages in case of ARPM controller for June 22, 2014.

Even lowering the threshold voltage, V_{th} (which is currently 1.058 p.u.) will not ensure that the voltage will be maintained below the upper limit of 1.058 p.u. as the load variation from one time step to another is unpredictable and can vary greatly. Fig. 3.2

represents the comparison of voltage profile for different V_{th} for one day (June 22). Though with V_{th} 1.04 p.u, the system was able to maintain the voltage, this will lead to much higher energy curtailment and energy loss in the system which is not desired. A lowered V_{th} is not desirable because of higher active power curtailment. Moreover, since the V-Q sensitivity (because R/X » 1) is low in distribution systems, the system will move to active power curtailment faster. Reducing the ramping time of reactive power absorption (t_{DQ}) could be one solution, however this may deteriorate the system dynamics because of sudden change in power.

An ideal inverter controller (used for overvoltage prevention in LV distribution system) should be able to prevent overvoltage without causing significant energy curtailment or loss in the distribution system. In the next section, impact on energy generation and consumption along with energy loss caused by each inverter controller implementation are compared.

3.2.2 Energy generation and loss

In Fig. 3.3, four different colored dots for each house illustrate the annual energy being generated by a house with four different inverter controllers for 2014. The bar graph of Fig. 3.4 represents the aggregated energy being generated by the 12 houses for different inverter controllers.

The total generated energy is greatest with the ARPM controller, because the ARPM controller uses latent reactive power capacity of the inverter as its first strategy to counter overvoltage; active power is curtailed only if absorbing maximum available reactive power by all houses is not sufficient to prevent the overvoltage. Among the

droop-based APC controllers, QDPAC produced the highest energy compared to LDAPC. By curtailing the active power proportional to the square of voltage deviation in QDAPC (instead of just the voltage deviation in LDAPC), less active power is curtailed when the voltage is near V_{cri}, allowing QDAPC to curtail less energy than LDAPC. OVP controller has least amount of energy generation because the inverter shuts down to prevent overvoltage, causing full curtailment of the available PV power. Additionally, the inverter remains off for five minutes after the overvoltage has occurred.

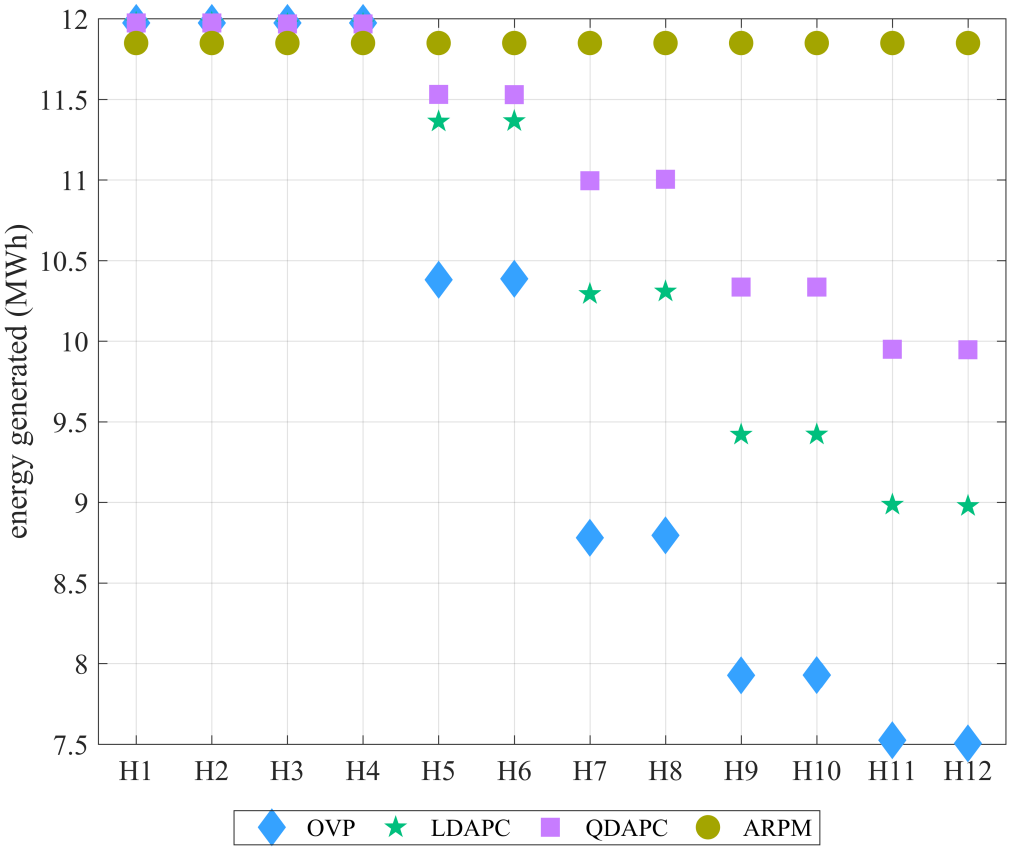

Figure 3.3. Housewise energy generation from PV for year 2014.

It is quite interesting to observe the fairness in energy generation from each of the 12 houses in case of ARPM controller. This is very important from the user point of view,

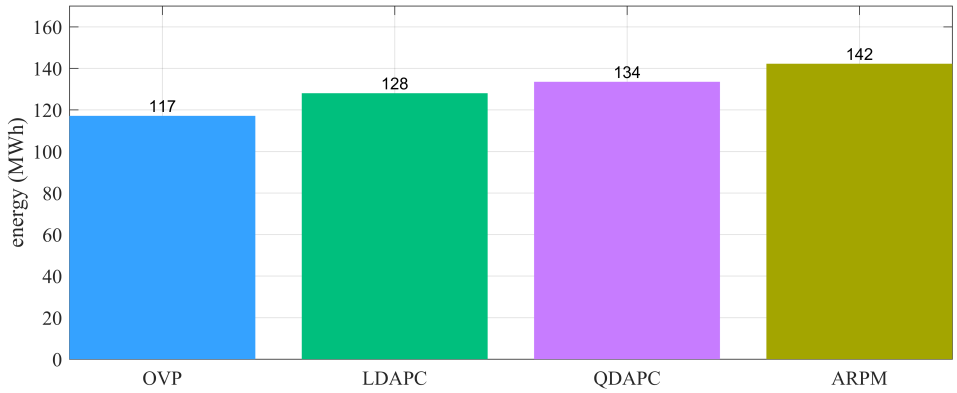

Figure 3.4. Controller-wise total energy generation for year 2014.

as energy generated is independent of the location of the house because of the coordinated reactive power absorption and active power curtailment strategy. This is not true for the other controllers as they make local decisions, which are greatly influenced by location on the network. The geographic location of house from the substation have impacts on the energy generation. This is because the increase in distance from substation results in increase in voltage.

Except ARPM, generation reduced greatly with the distance from the transformer in other controllers (note, H1 is the nearest house and H12 is the farthest house from the substation, shown in Fig. 2.3). On the other hand, total energy generated by houses close to the substation transformer (specifically, H1 – H4) are the same with OVP, LDAPC and QDAPC inverter controllers, with a slight reduction in energy generation with ARPM controllers (caused by coordinated active power curtailment, where houses may curtail before they have a local voltage issue). This may discourage end-users living close to the transformer from using the ARPM controller, but the overall system benefit is greater (and more fair) which will encourage more PV installation, regardless of network location.

The local generation of energy using PV helps in reducing the demand or consumption of electricity. In Fig. 3.5, each dot represents the net energy consumed by the house with different colors for different inverter controllers for 2014 (except for blue colored dots, which represents energy consumption without PV). The bar graph in Fig. 3.6 represents the aggregated energy consumption of all 12 houses compared to the no PV case for the same year.

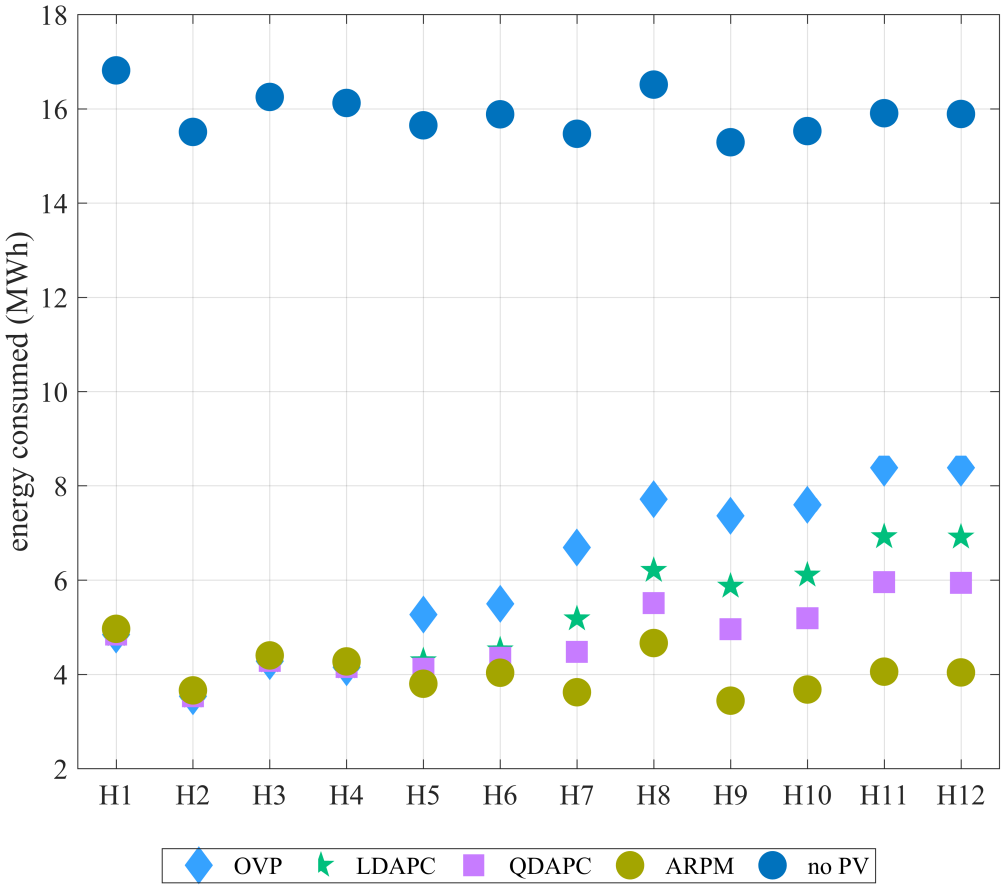

Figure 3.5. House-wise net annual energy consumption.

The total energy consumption is least when using the ARPM controller, whereas it is the greatest in OVP. This is because of the highest energy is being generated with ARPM controller and the least with OVP as shown in Fig. 3.4. The reduced energy consumption

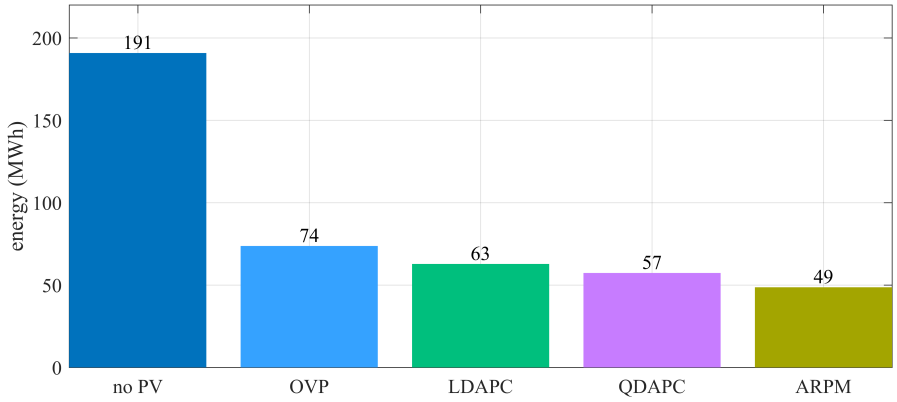

Figure 3.6. Controller-wise total energy consumption.

with QDAPC compared to LDAPC can be explained similarly using the argument of higher generation. The energy consumed decreased greatly with the installation of PV in all houses, directly leading to economic benefits for the owner. The similar nature of energy consumption between no PV case and with ARPM controller in all houses resembles fairness in the reduction of consumption. The difference in energy consumed in the no PV case is from the randomness of the load generation from the queue model.

Energy loss is another pertinent aspect to be analyzed to access the performance of the overvoltage prevention inverter controllers. In Fig. 3.7, the annual curtailed energy with 12 house combined (energy not being injected to prevent overvoltage) is compared with distribution system losses for different inverter controllers for 2014. The distribution system energy losses includes transformer losses and the distribution line losses.

The curtailment is highest with OVP controller. This is because, the inverter curtails full PV power once the overvoltage is experienced at its point of connection in this control method. Energy loss is another pertinent aspect to be analyzed to assess the performance of the overvoltage prevention inverter controllers. In Fig. 3.8, the annual distribution

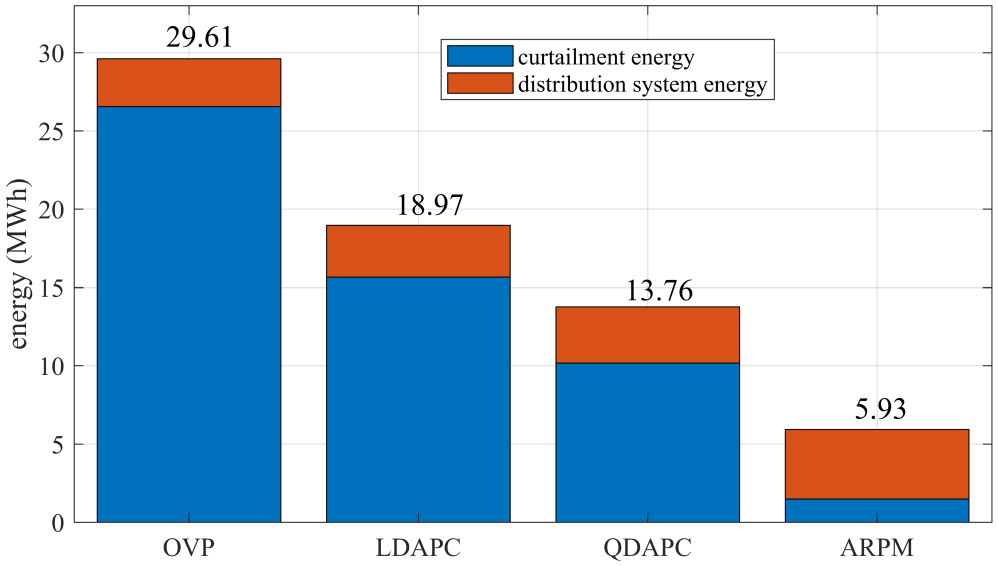

Figure 3.7. Annual energy loss due to curtailment and distribution system feeder loss for different types of PV inverter controller.

system losses for different inverter controllers for 2014 are shown, compared to the case with no PV. The distribution system energy losses are divided into transformer losses and the distribution line losses. The transformer losses only include the equivalent series impedance. Actual transformer losses will be slightly as shunt parameters are neglected. However, this will not affect the comparison study, because the change in no-load loss due to the controllers is insignificant compared to the change in series losses. The higher distribution energy loss in case of ARPM controller compared to the rest of the three controllers is due to higher active power injection and higher reactive power absorption. Transformer losses contributed to almost 40% of the total distribution loss in the system. The higher energy loss in droop-based APC controllers (both LDAPC and QDAPC) than OVP is because of the higher energy being injected from PV by these controllers.

In the no PV case, the total distribution energy loss is lower compared to the

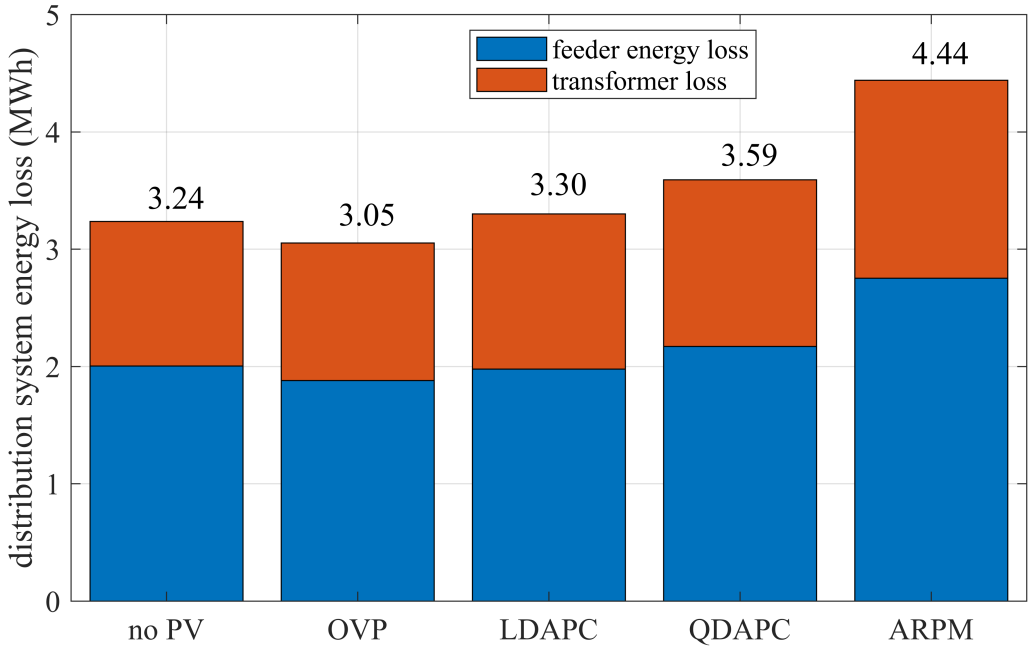

Figure 3.8. Distribution system feeder loss in transformer and distribution line for different types of PV inverter controller.

LDAPC, QDAPC, and ARPM, but is slightly higher than the OVP control method. This can be explained by using two arguments. First, losses in the distribution system during the no PV case is caused only by the unidirectional power flow from the substation to the end-user, while after installing PV distribution system losses include losses due to bidirectional power flow. Second, the contribution to distribution system losses during reverse flow is dependent on the amount of net power being injected, (higher injection leads to higher loss). The higher total energy loss in the distribution system with no PV compared to OVP is cannot be generalized and might differ for different loading, irradiance data, and PV installation.

This energy loss, along with reactive power absorbed in the feeder, must be supplied through the distribution transformer, significantly affecting the transformer loading. The next section discusses the increased transformer loading for different inverter controllers.

3.2.3 Impact on distribution transformer loading

A kernel density estimate of apparent power loading of the distribution transformer $\hat{f}_{kVA}$ from the random sample kVA_1, kVA_2,.....,kVA_n of size n for bandwidth or smoothing parameter h, can be written as [31],

$$\hat{f}_{kVA} = \frac{1}{nh}\sum_{i=1}^{n} K(\frac{kVA - kVA_i}{h}) \tag{3.3}$$

where K is the kernel density function that integrates to 1. A normal kernel density function used for estimation of $\hat{f}_{kVA}$ (note any kernel density estimator can be used) because of its simplicity. So function K(x) is standard normal density defined as,

$$K(x) = \frac{1}{\sqrt{2\pi}} e^{-\frac{1}{2}x^2} \tag{3.4}$$

The bandwidth is selected based on the Silvermans rule of thumb [32] which is given as,

$$h \approx 1.06\hat{\sigma}n^{-1/5} \tag{3.5}$$

where $\hat{\sigma}$ is the standard deviation of kVA data samples. Similarly the normal kernel density function for active power (kW) and reactive power (kVar) can be evaluated. The impact of the different PV controllers on apparent power, active power and reactive power loading of the distribution transformer is shown in Fig. 3.9 as a kernel density estimation. The figure shows how often the distribution transformer had a apparent power loading (in kVA), active power (kW), and reactive power (kVar) throughout the annual simulation for

each controller compared to the no PV case. The transformer's apparent power seems to be under utilized with no PV, indicated by the red curve (i.e., oversized). With the addition of of PV in the distribution system, the transformer at times is loaded near full capacity. Droop-based APC control methods loaded the transformer to 60 kVA at times (at a rated capacity of 75 kVA), at which point all active power, as shown in the figure, would be curtailed based on voltages reaching the threshold. The higher density for higher apparent power loading with ARPM controller indicates the higher chances of utilizing the transformer near full capacity, due to the reduced active power curtailment, with increased reactive power absorption(as shown in the figure with reactive power kernel density estimation). The OVP control though was better than the no PV case in terms of pushing the transformer loading towards the full capacity but is not as good as the other inverter controllers in this study. This is because of the inability of OVP to maintain the PV injection near threshold voltage. Analysis of the apparent power loading of the transformer is important to ensure that the transformer is not overloaded. The active power loading of the transformer during the reverse power flow directly impacts the financial benefit of the end-users. It is found that when PV is used, the transformer can be reverse loaded in terms of active power up to 60 kW. The reactive power loading of the transformer will be similar for OVP, LDAPC, and QDAPC compared to no PV case because none of these controllers are using reactive power for overvoltage protection. However, with the ARPM controller, higher reactive power loading (and therefore higher system losses) is expected due to the use of the reactive power absorption capability of the inverter.

The analysis up to now presents the technical impact of inverter controllers described in 2.1. The following subsection is focused on analyzing long term economic

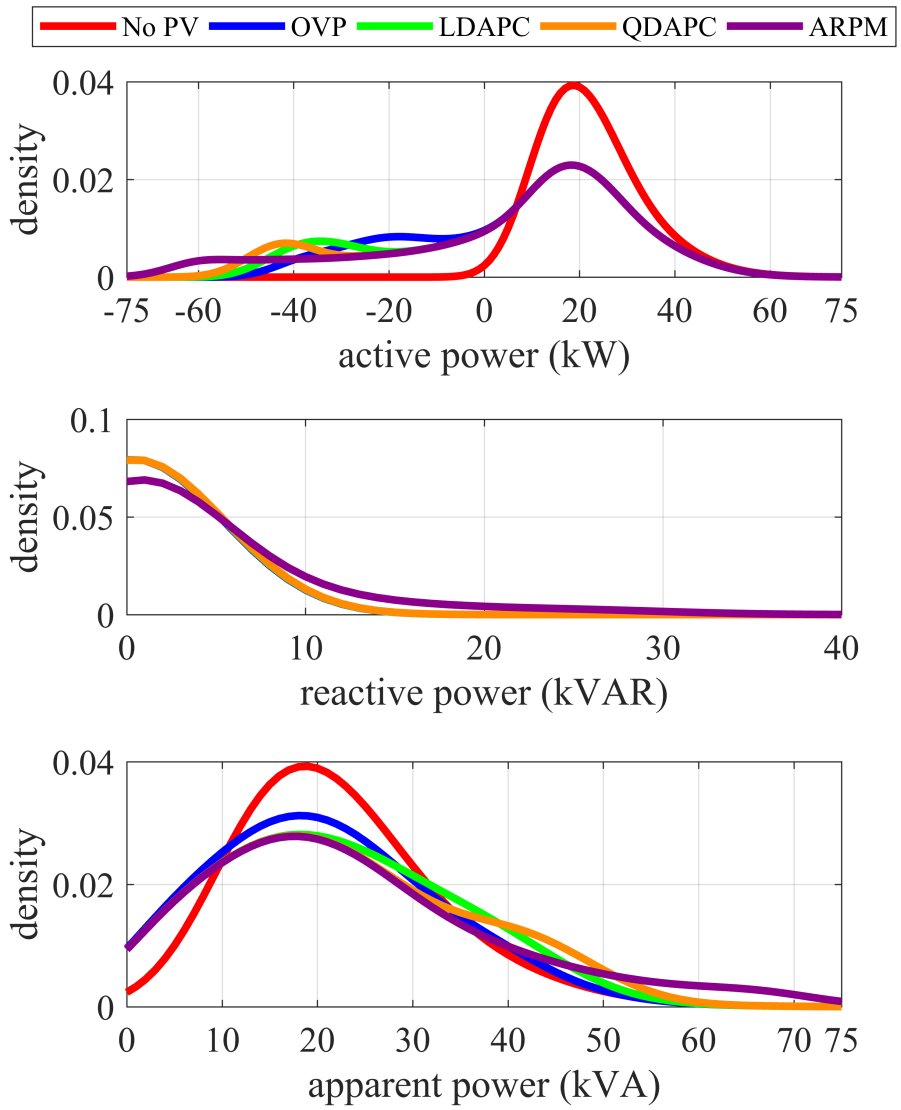

Figure 3.9. Kernel density function for active power, reactive power and apparent power loading of 75 kVA transformer for 2014.

impact of overvoltage prevention inverter controllers using two different pricing structures, specifically real-time price & flat rate tariff.

3.2.4 Financial impact on utility, government, and customers

The analysis up to now presents the technical impact of the inverter controllers. In this section, the long-term economic impact of overvoltage prevention inverter controllers is analysed using two different pricing structures, specifically RTP and flat rate tariff. The

electricity tariff scheme has a significant impact on the financial benefit of the end-user, utility, and government. The electricity charges paid by the end-user can be split into three major categories: supply charges, distribution charges, and taxes and fees as described in Section 3.1.4. The electric utility, such as ComEd, gains benefit from distribution charges paid by the end-user. Government and energy agencies gets direct benefit from taxes and fees that end-user pay for consuming the electricity. The supply charges go to the regional transmission organization (RTO)/independent system operator (ISO), such as PJM, which operates the wholesale electricity market.

In Fig. 3.10, each marker represents the electricity bill incurred for a house, with the different colors and shapes indicating different inverter controllers (or no PV) using RTP pricing with net-metering. For this study, it is assumed that end-users do not deviate their consumption pattern based on the RTP (e.g., demand response of the consumer). A similar figure shown in 3.11 is generated using fixed rate tariff instead of RTP. The charge paid by the house after the installation of PV decreased greatly in all houses. The reduction in electricity bill for a house closer to the substation (specifically H1, H2, H3, H4) remains almost unaffected for OVP, LDAPC, and QDAPC control method, with a slightly higher electricity bill with ARPM in both tariff schemes. This is because houses H1 - H4 never curtail active power with OVP, LDAPC, and QDAPC controllers (refer to voltage profile section) whereas the ARPM controller forces some houses to participate in active power curtailment even if their local voltage does not exceed V_{th}. The other important observation is that houses far from the substation have considerable difference in their electricity bill reduction depending on the type of inverter control method employed with similar nature in both RTP and fixed rate tariff. This is because houses closer to the

substation have lower chances of experiencing overvoltage than those far from the substation as discussed earlier. The reduction in electricity bill incurred is in the increasing order OVP, LDAPC, QDAPC, and ARPM for houses located far from the substation (H5 to H12), because the energy generation increases in the same order (refer to Fig. 3.4).

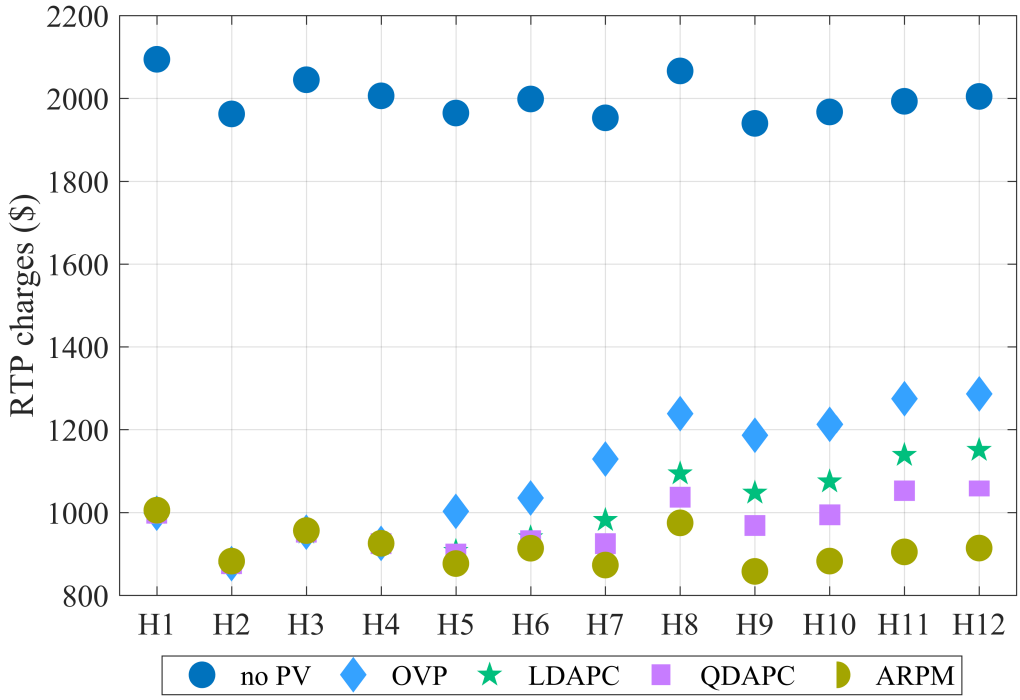

Figure 3.10. Annual electric utility charge for each house with different types of PV inverter controller for RTP.

The aggregated annual electricity bill incurred from all 12 houses is shown with grouped bar graph in Fig. 3.13. It is interesting to observe nearly identical electricity bills for both the RTP and flat rate tariff schemes when there in no PV installation in the system, implying that ComEd designed the RTP in such a way that the overall benefit gained by the utility remains almost unaffected whether end user chooses RTP or flat rate tariff if no PV is installed and the end-user does not change their consumption behavior in response to the price. Because the total generation energy with 12 house combined is in

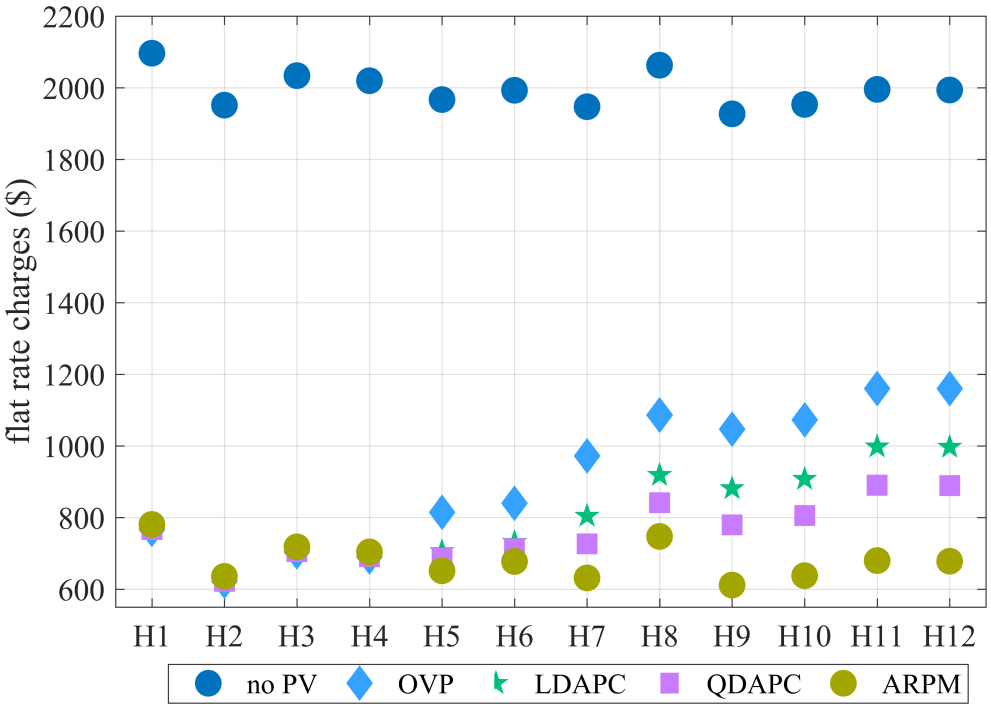

Figure 3.11. Annual electric utility charge for each house with different types of PV inverter controller for flat rate tariff.

the increasing order OVP, LDPAC, QDAPC, and ARPM, the difference in total electricity bill paid using two pricing schemes will increase in the same order.

The aggregated annual electricity bill is lower for flat rate tariff in all inverter controllers because the net metering received from injected active power is higher during high PV generation, as shown in Fig. 3.12. In Fig. 3.12, the blue line shows the variation of transformer active power (negative for generation, and positive for consumption) with the ARPM controller. The solid orange line represents the RTP, and the dotted line represents the flat rate tariff for June 22, 2014. It is seen that the RTP is less than flat rate when the houses generate the most PV power due to the load/price peak and the solar peak not aligning. This will motivate the end-user with PV to either (i) adopt the flat rate tariff to gain more benefit from their PV, or (ii) adopt a load/battery management system to

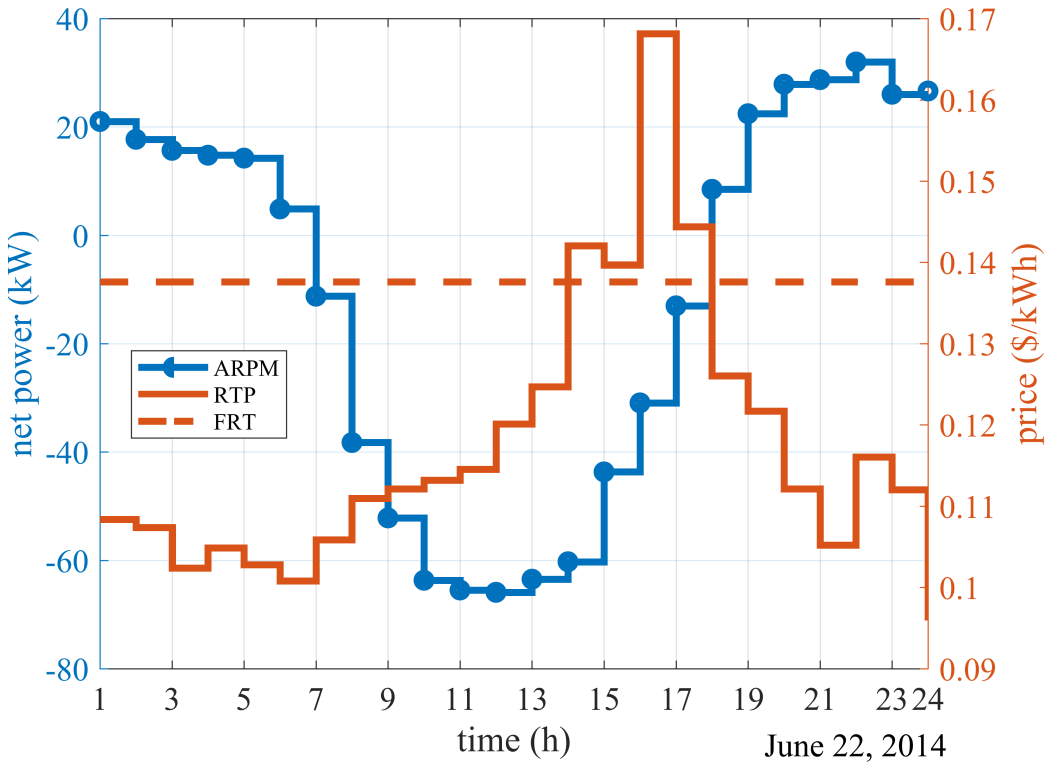

Figure 3.12. Right Y-axis: Comparision of RTP and flat rate tariff prices for a day of June 22, 2014. Left Y-axis: Net transformer power profile with different types of PV inverter controller for a day of June 22, 2014.

better coordinate PV, load, and price. The variation of net transformer active power is similar for the other three inverter controllers, however with different magnitudes.

As the different controllers directly impact the economic benefit of PV, the payback period of PV installation is also impacted. Figure 3.14 shows the simple payback period (computed by dividing the PV installation cost by the yearly income from PV) for the nearest (H1) and farthest (H12) house from the transformer for four different PV inverter controllers with RTP and flat rate tariff pricing schemes for the 8.4 kW PV considered in the study. The cost of PV system installation is chosen to be $3.22/watt [33]. As the flat rate tariff is higher than RTP during peak PV generation, the payback period will be shorter for flat rate when using net metering, regardless of the controllers for both houses.

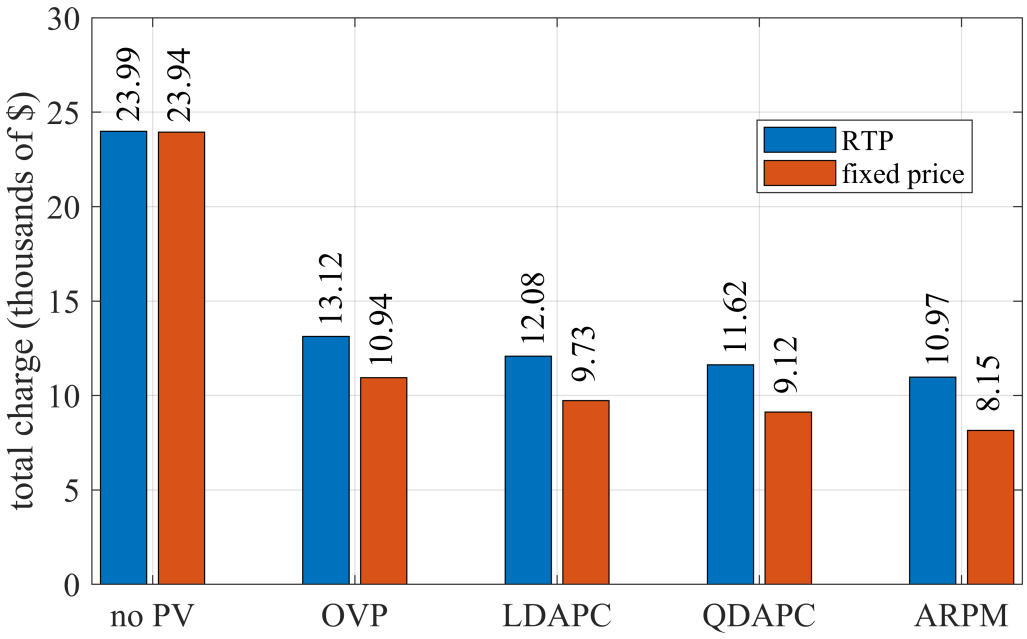

Figure 3.13. Comparision of electric utility bill for RTP and flat rate tariff for different types of PV inverter controller.

Similarly, since ARPM control method can allow inverter to inject more active power, the payback period will be reduced compared to the other three control methods, regardless the type of tariff scheme adopted. For a given control method (among OVP, LDAPC, and QDAPC), because the nearest house (H1) can inject more energy than the farthest house (H12), H1 will have a shorter payback period than H12 for the same tariff scheme. However with ARPM, as every house curtails the same amount of active power, all houses will have similar payback periods (with variations coming from the different load).

Fig. 3.15 shows the net utility benefit with different PV inverter controllers schemes and also without PV considering distribution loss in orange bars and neglecting distribution loss in blue bars. The overlayed bar graph within the Fig. 3.15 represents cost associated with losses in the distribution system and is to be paid by the utility. To compute the net benefit to the utility, delivery charges from both (RTP and flat rate)

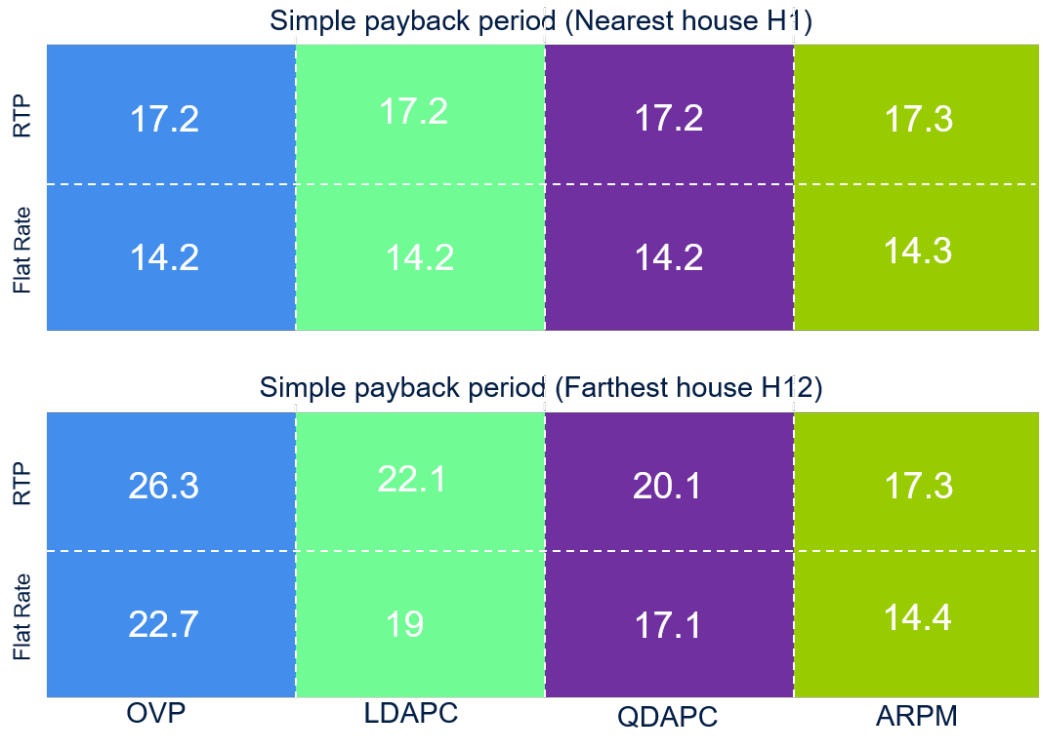

Figure 3.14. Payback period for 8.4 kW PV system for different PV inverter controller.

bills [27] have been considered (note, supply charges and taxes and fees do not contribute to the utility benefit). As the utility has to pay for losses in the feeder and transformer, the net utility benefit is reduced when considering losses in all controller schemes. The net benefit gained decreased in the order OVP, LDAPC, QDAPC, and ARPM. This reduction is mainly caused by reduced total energy consumption due to the increased local power production using PV by the houses. The increased cost of losses from the ARPM controller are due to higher reactive power absorption from PV houses to control the overvoltage (ultimately supplied by the distribution transformer).

The policy of net metering for houses with PV is highly beneficial to the PV consumer, but the lost revenue of the utility may lead to increased electricity prices for non-PV consumers to recoup lost capital and maintenance costs involved with the

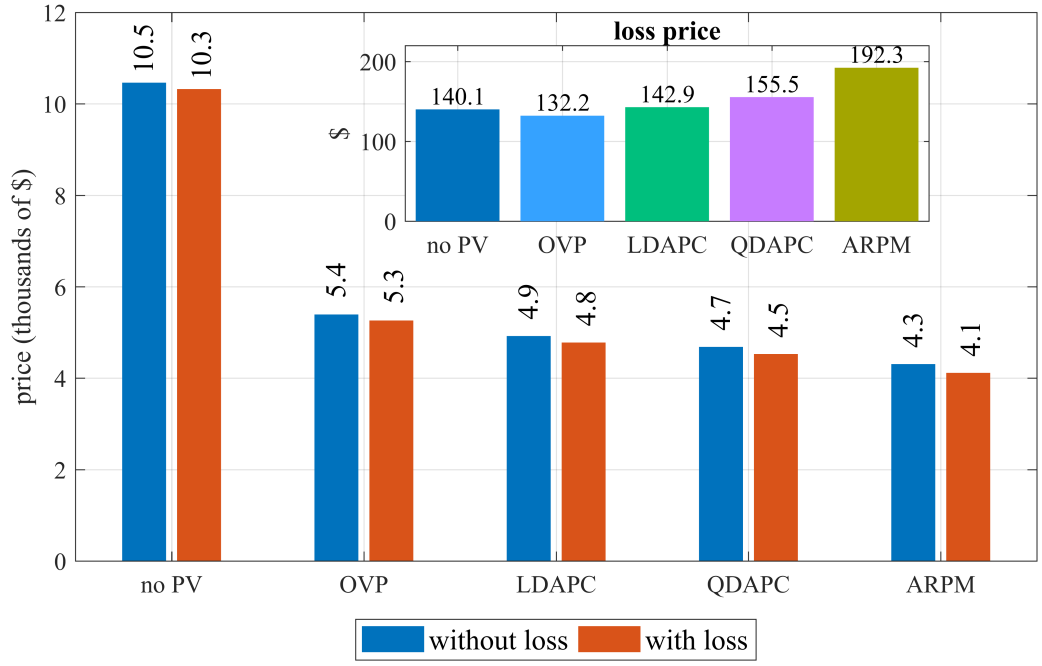

Figure 3.15. Utility benefit (electric sales minus energy purchase from ISO) with and without considering distribution system losses (higher is better for ComEd). The top-right box gives the cost of distribution system losses for the different types of PV inverter controllers.

distribution system. If the price of electricity goes up, the non PV user may then install PV to reduce their electricity consumption from utility, further reducing the electricity sold by the utility. The cumulative effect of such events may lead to a *utility death spiral* [34], a situation where utility existence is under threat due to the continued decline of net electricity sales from the utility. The effect of tariff structures on death spiral of utility is however, out of the scope of this thesis.

To show the impact on government and agencies working for social benefit, the taxes and fees for the end-user is shown for different inverter controllers in Fig. 3.16 using two different pricing structures (RTP and flat rate tariff). The annual aggregated taxes and fees paid by the 12 houses decreased in the order OVP, LDAPC, QDAPC, and ARPM for

both tariff schemes because of reduced energy consumption by end-users in the same order. Similarly, the total taxes and fees paid by the 12 house is lower for RTP compared to flat rate tariff because of higher flat rate during high PV generation. This suggests that the benefit to the government and utility decreases when using more effective (in a sense of lower total energy curtailment) inverter overvoltage prevention control methods.

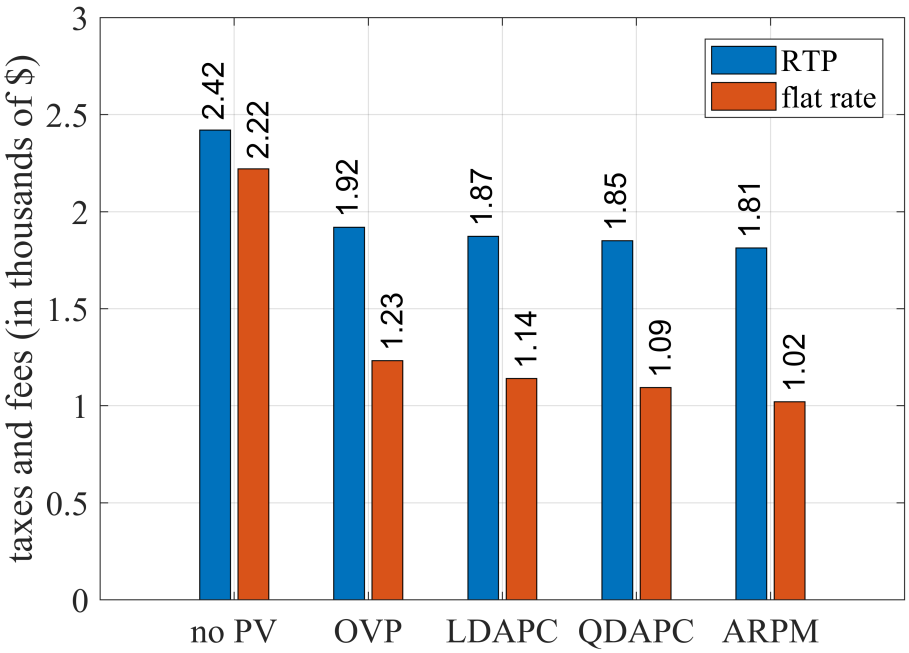

Figure 3.16. Taxes and fees charges for different PV inverter controller for RTP and flat rate tariff.

CHAPTER 4 DEVELOPMENT OF 216 HOUSE LARGE DISTRIBUTION FEEDER IN GRIDLAB-D

The increasing number and size of photovoltaic (PV) systems at the distribution system level has resulted in an increased interest in distribution system modeling for use in determining the impacts of such PV integration. Accordingly, many distribution system modeling tools have been developed to evaluate and quantify these impacts. One of the desirable features of modeling tools is the ability of the tools to investigate the operational characteristics of a modeled distribution system and an interconnected PV system over a set time period (typically from sub-second to many years). This type of analysis, called quasi-static time-series (QSTS) analysis is typically used to evaluate the long term impact of a large distribution system (with three phase system with several number of houses). The advantage of QSTS over tradition differential-based solvers is that it is not necessary to integrate all the device's behaviors into a single set of equations that must be solved.

4.1 Benchmark

A typical low voltage distribution feeder adopted from [18] with total 216 number of houses, 72 houses in each phase as shown in Fig. 4.1. The three phase, 94 MVA, 120 kV - 25 kV substation transformer supply power to three phase and single phase lumped load as well as the 216 houses. A constant balanced load of 60 MVA operating at power factor of 0.95 lagging is connected in the substation. The transformer at the substation are equipped with an on-load tap changer on the secondary winding +/-10 % voltage variation over 32 steps.

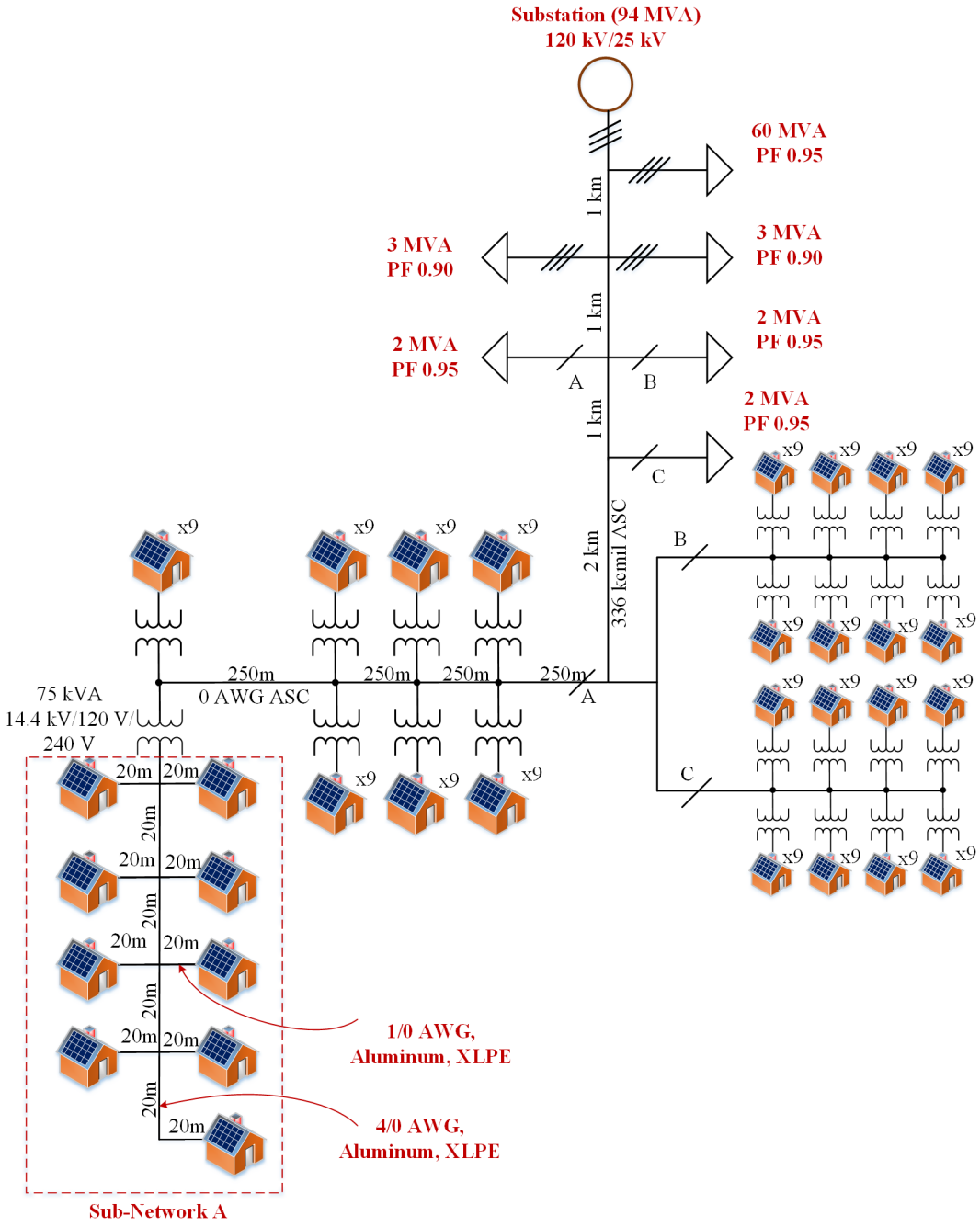

Figure 4.1. 216 house benchmark system under consideration.

The voltage set point in the on-load tap changer is adjusted to 1.03 pu and the control bandwidth is 2 % of the rated voltage. A 25 kV overhead distribution feeder wired with 336 kcmil, all aluminum stranded conductors (ASC) is extended up to 5 km and

end-up to a three individual neighbourhood with phase A,B and C. The distribution laterals wired with 0 AWG ASC are connected at 1 km, 2 km, 3 km, and 5 km from the substation. At 1 km from the substation, two 3 MVA , three phase loads operating at 0.9 power factor is distributed over 1 km. At 2 km from the substation, two 2 MVA, single-phase (A and B) loads operating at 0.95 power factor is distributed over 2 km. At 3 km from substation, one 2 MVA, single phase (C) load operating at 0.95 power factor is distributed over 2 km. At 5 km from the substation, the three phase feeder is split into three one phase laterals consisting neighbourhood. Each lateral is extend up to 1 km and has eight 75 kVA single-phase 14.4 kV - 120/240 V distribution transformer distributed at 0.25 km distance. The secondary circuit of the distribution transformer is 80 m of cable of type NS90 consisting of two live wire twisted around the neutral cable. There are nine customers with eight connected in pairs in every 20 m with last customer connected separately. The service entrance wire is a length of 20 m consisting two wires supported by a steel grounded neutral cable. Each house in each phase is composed of grid connected PV with a capacity of 8.4 kW. The details of single phase, three phase and transformer parameter are given in appendix in Table D.1, D.2, and D.3 respectively.

4.2 Feeder validation in PSCAD and GridLAB-D

The 216 house benchmark system is modeled in Electromagnetic transient simulation software, PSCAD and Quasi steady times series software, GridLAB-D.

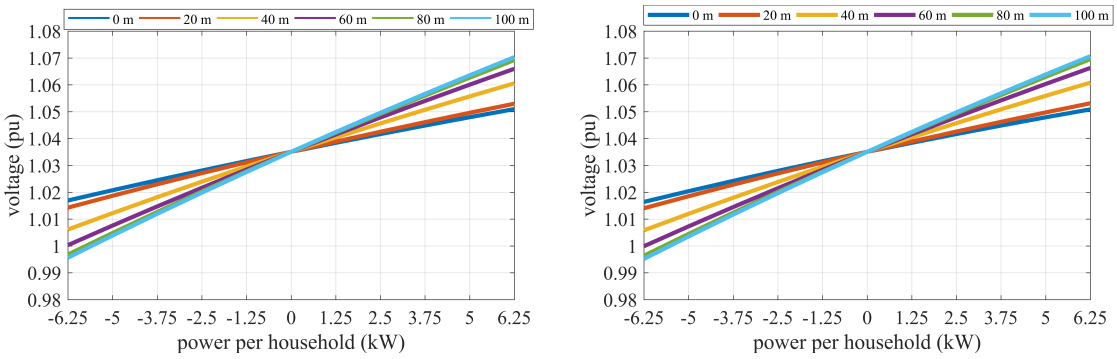

Figure 4.2. Voltage profile in low voltage side (a) simulated in GridLAB-D (b) simulated in PSCAD.

The voltage profile for different house power for both of the simulation softwares is measured on the low voltage and high voltage side. The voltage at low voltage side is measured at 0 m (secondary of transformer), 20 m 40 m, 60 m 80 m and 100 m. In case of medium voltage, the voltage is measured at 0 km (substation), 1 km, 2 km, 3 km, 5 km and 6 km from substation. The voltage profile measured both in PSCAD and GridLAB-D at the low voltage side with varying power at each house from 6.25 of net load to 6.25 of net generation is shown in Fig. 4.2 (a) and (b).

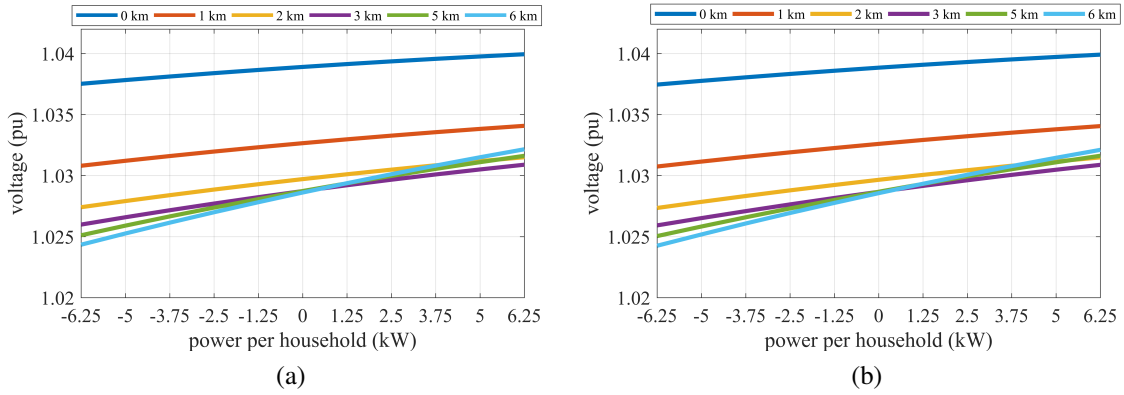

Figure 4.3. Voltage profile in medium voltage side (a) simulated in GridLAB-D (b) simulated in PSCAD.

The voltage profile measured both in PSCAD and GridLAB-D at the medium voltage side with varying power at each house from 6.25 of net load to 6.25 of net generation is shown in Fig. 4.3 (a) and (b).

The error calculated between the voltage of two simulation software in low voltage side is shown in Fig. 4.4 (a). Similarly, the voltage error between the voltage of two simulation software in medium voltage side is shown in Fig. 4.4 (b). The small error between the two simulation software might be modelling difference between two different types of simulation software.

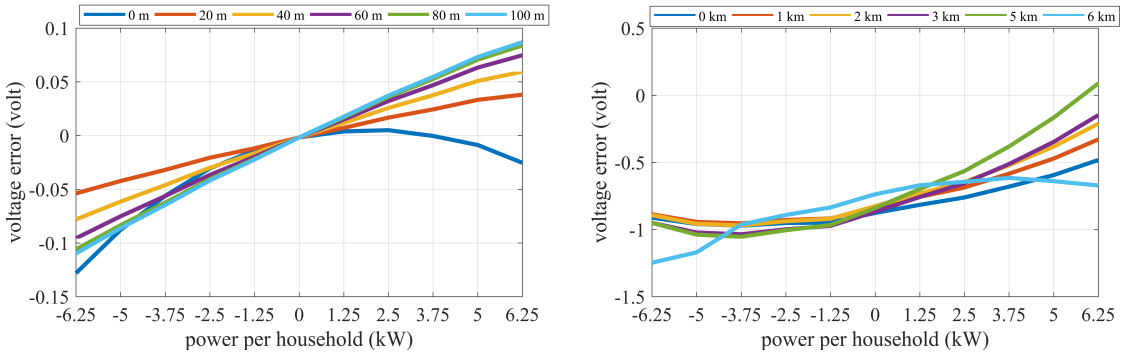

(a) (b)

Figure 4.4. Voltage error between GridLAB-D and PSCAD (a) low voltage side (b) medium voltage side.

CHAPTER 5 CONCLUSIONS

5.1 Conclusions

This research work presented the development of a framework for evaluating long-term techno-economic analysis of any PV inverter control method, and included a year-long example comparing three methods. The different types of PV inverter controllers are compared in an electric distribution system model developed in a QSTS simulator. The challenge and a solution for numerical oscillations when using a QSTS simulator was overcome by the design of a sensitivity-based algorithm. An annual simulation study for the year 2014 in Chicago, IL, for PV inverter controllers was performed in terms of voltage control, energy generation and curtailment, feeder losses, and end-user, government, and utility economic impacts. Droop-based active power curtailment (LDAPC and QDAPC) inverter controllers were shown to be simple and effective local overvoltage prevention methods that guarantee overvoltages are not caused by PV systems. However, the results showed that using the reactive power capability of inverters for overvoltage prevention outperforms methods that only consider active power curtailment. While using reactive power does helps in overvoltages prevention, this method also increases system losses and further reduces electric sales from the utility, decreasing the utilities net revenue.

Appendix A. Electrical distribution network parameter for 12 house system

The single-phase line parameter of the feeder are given in Table A.1. Table A.2 provides the low voltage transformer parameter.

Table A.1. Single-phase PI section lines parameter (per line conductor).

	Drop Lines	Pole-Pole Lines
R	0.549 Ω / km	0.346 Ω / km
L	0.23 mH / km	0.24 mH / km
C	0.055 μF / km	0.072 μF / km

Table A.2. LV transformer parameter.

S	75 kVA	$R_{2,3}$	0.012 pu
V_1	14.4 kV	$L_{2,3}$	0.025 pu
R_1	0.006 pu	R_m	500 pu
L_1	0.02 pu	L_m	500 pu
$V_{2,3}$	120 V		

Appendix B. Electric bill

Electric bill for RTP and flat rate tariff are given in table:

Table B.1. Supply Charge

		RTP scheme	Flat rate scheme
Supply charges	Electricity supply charges (per kWh)	*	$0.05865
	Transmission services charge (per kWh)	$0.00844	$0.01122
	Capacity charge (per kW)	$4.69477	-
	Msc procurement component charge (per kWh)	$0.0011	-
* can vary hourly available online [29]			

Table B.2. Delivery Charge

		RTP scheme	Flat rate scheme
Delivery charges	Customer charge	$11.55	$10.53
	Standard metering charge	$4.68	$4.36
	Distribution facilities charge (per kWh)	$0.03484	$0.03156
	Illinois electricity distribution charge (per kWh)	$0.00118	$0.00116

Table B.3. Taxes and Fees

		RTP scheme	Flat rate scheme
Taxes & fees	Environmental cost recovery adj (per kWh)	$0.00026	$0.00038
	Renewable portfolio standard (per kWh)	$0.00094	$0.00189
	Zero emission standard (per kWh)	$0.00196	$0.000195
	Franchise cost (% of delivery charge)	1.92%	2.363%
	Energy efficiency programs (per kWh)	-	$0.00345
	State tax [30] (¢/ kWh)	0.33	0.33
	Municipal tax [30] (¢/ kWh)	0.46	0.46

Appendix C. Sensitivity

The sensitivity of the power network is amount of change of voltage per unit change in active power. For a 12 house network, change in voltage due to changes in power in each node can be obtained by 12×12 sensitivity matrix [20] which is given by (C.1).

$$\frac{\Delta V_{Hi}}{\Delta P_{Hj}} = \begin{bmatrix} 0.0509 & 0.0509 & 0.0486 & 0.0486 & 0.0468 & 0.0468 & 0.0455 & 0.0455 & 0.0447 & 0.0447 & 0.0442 & 0.0442 \\ 0.0509 & 0.0509 & 0.0486 & 0.0486 & 0.0468 & 0.0468 & 0.0455 & 0.0455 & 0.0447 & 0.0447 & 0.0442 & 0.0442 \\ 0.0510 & 0.0510 & 0.1055 & 0.1055 & 0.1025 & 0.1025 & 0.1002 & 0.1002 & 0.0988 & 0.0988 & 0.0981 & 0.0981 \\ 0.0510 & 0.0510 & 0.1055 & 0.1055 & 0.1025 & 0.1025 & 0.1002 & 0.1002 & 0.0988 & 0.0988 & 0.0981 & 0.0981 \\ 0.0510 & 0.0510 & 0.1056 & 0.1056 & 0.1595 & 0.1595 & 0.1564 & 0.1564 & 0.1543 & 0.1543 & 0.1532 & 0.1532 \\ 0.0510 & 0.0510 & 0.1056 & 0.1056 & 0.1595 & 0.1595 & 0.1564 & 0.1564 & 0.1543 & 0.1543 & 0.1532 & 0.1532 \\ 0.0510 & 0.0510 & 0.1056 & 0.1056 & 0.1596 & 0.1596 & 0.2136 & 0.2136 & 0.2109 & 0.2109 & 0.2095 & 0.2095 \\ 0.0510 & 0.0510 & 0.1056 & 0.1056 & 0.1596 & 0.1596 & 0.2136 & 0.2136 & 0.2109 & 0.2109 & 0.2095 & 0.2095 \\ 0.0510 & 0.0510 & 0.1056 & 0.1056 & 0.1596 & 0.1596 & 0.2136 & 0.2136 & 0.2682 & 0.2682 & 0.2666 & 0.2666 \\ 0.0510 & 0.0510 & 0.1056 & 0.1056 & 0.1596 & 0.1596 & 0.2136 & 0.2136 & 0.2682 & 0.2682 & 0.2666 & 0.2666 \\ 0.0510 & 0.0510 & 0.1056 & 0.1056 & 0.1596 & 0.1596 & 0.2136 & 0.2136 & 0.2682 & 0.2682 & 0.3241 & 0.3241 \\ 0.0510 & 0.0510 & 0.1056 & 0.1056 & 0.1596 & 0.1596 & 0.2136 & 0.2136 & 0.2682 & 0.2682 & 0.3241 & 0.3241 \end{bmatrix} \left[\frac{V}{kW}\right] \tag{C.1}$$

where, $i = 1,2,3,...12$ and $j = 1,2,3,...12$. Each element in this matrix is to be interpreted as the variation that would happen in the voltage profile in a certain bus i in the case of a hypothetical 1 p.u. variation in the injection of active power in bus j. Maximum value in each row occur at diagonal element suggests that the voltage will vary significantly with power variation in same bus as compared to power variation in other bus.

Appendix D. Electrical distribution network parameter for 216 house system

Table D.1. Single-Phase PI section lines parmeter (Per line conductor)

	Drop Lines	Pole-Pole Lines	Laterals
R	0.549 Ω / km	0.27 Ω / km	0.535Ω / km
L	0.23 mH / km	0.24 mH / km	1.33 mH / km
C	0.055 μF / km	0.072 μF / km	4.3 nF / km

Table D.2. Three-Phase PI section lines parameters

	336 kcmil Line with 2/0 Neutral ASC	# 0 Line with #0 Neutral
R_1	0.1902 Ω / km	0.603 Ω / km
L_1	1.09 mH / km	1.213 mH / km
C_1	11 nF / km	9.90 nF / km
R_0	0.5271 Ω / km	0.978 Ω / km
L_0	3.37 mH / km	3.639 mH / km
C_0	4.9 nF / km	4.73 nF / km

Table D.3. Transformer parameter

	Low voltage Transformers	Substation Transformer
S	75 kVA	47 MVA
V_1	14.4 kV	120 kV
R_1	0.006 pu	0.005 pu
L_1	0.02 pu	0.0924 pu
$V_{2,3}$	120 V	25 kV
$R_{2,3}$	0.012 pu	0.005 pu
$L_{2,3}$	0.025 pu	0.0924 pu
R_m	500 pu	500 pu
L_m	500 pu	500 pu

REFERENCES

[1] L. Sherwood, *U.S. solar market trends 2013*, July 2014. [Online]. Available: https://irecusa.org (visited on 04/14/2018).

[2] P.-C. Chen, R. Salcedo, Q. Zhu, F. De Leon, D. Czarkowski, Z.-P. Jiang, V. Spitsa, Z. Zabar, and R. E. Uosef, "Analysis of voltage profile problems due to the penetration of distributed generation in low-voltage secondary distribution networks," *IEEE Transactions on Power Delivery*, vol. 27, no. 4, pp. 2020–2028, Oct. 2012.

[3] ANSI C84.1, *Voltage Rating for Electric Power Systems and Equipment*, 1989.

[4] C. L. Masters, "Voltage rise: the big issue when connecting embedded generation to long 11 kV overhead lines," *Power Engineering Journal*, vol. 16, no. 1, pp. 5–12, Feb. 2002.

[5] S. Cobben, B. Gaiddon, and H. Laukamp, "Impact of Photovoltaic Generation on Power Quality in Urban Areas with High PV Population - Results from Monitoring Campaigns," Tech. Rep., 2008, pp. 1–53. [Online]. Available: http://pvupscale.org/IMG/pdf/WP4_D4-3_public_v1c.pdf.

[6] Y Ueda, K Kurokawa, T Tanabe, K Kitamura, and H Sugihara, "Analysis results of output power loss due to the grid voltage rise in grid-connected photovoltaic power generation systems," *IEEE Transactions on Industrial Electronics*, vol. 55, no. 7, pp. 2744–2751, Jul. 2008.

[7] D. Cheng, B. A. Mather, R. Seguin, J. Hambrick, and R. P. Broadwater, "Photovoltaic (PV) impact assessment for very high penetration levels," *IEEE Journal of Photovoltaics*, vol. 6, no. 1, pp. 295–300, Jan. 2016.

[8] M. E. Elkhatib, R. El-Shatshat, and M. M. A. Salama, "Novel Coordinated Voltage Control for Smart Distribution Networks With DG," *IEEE Transactions on Smart Grid*, vol. 2, no. 4, pp. 598–605, Dec. 2011.

[9] O. Homaee, A. Zakariazadeh, and S. Jadid, "Real-time voltage control algorithm with switched capacitors in smart distribution system in presence of renewable generations," *International Journal of Electrical Power & Energy Systems*, vol. 54, pp. 187 –197, Jan. 2014.

[10] R. Kabiri, D. G. Holmes, B. P. McGrath, and L. G. Meegahapola, "LV Grid Voltage Regulation Using Transformer Electronic Tap Changing, With PV Inverter Reactive Power Injection," *IEEE Journal of Emerging and Selected Topics in Power Electronics*, vol. 3, no. 4, pp. 1182–1192, Dec. 2015.

[11] Y. Wang, P. Zhang, W. Li, W. Xiao, and A. Abdollahi, "Online overvoltage prevention control of photovoltaic generators in microgrids," *IEEE Transactions on Smart Grid*, vol. 3, no. 4, pp. 2071–2078, Dec. 2012.

[12] R. Tonkoski, L. A. Lopes, and T. H. El-Fouly, "Coordinated active power curtailment of grid connected PV inverters for overvoltage prevention," *IEEE Transactions on Sustainable Energy*, vol. 2, no. 2, pp. 139–147, Apr. 2011.

[13] M. Maharjan, "Voltage regulation of low voltage distribution networks," M.S. Thesis, South Dakota State University, 2017, pp. 1–81.

[14] P. Jahangiri and D. C. Aliprantis, "Distributed Volt/VAr control by PV inverters," *IEEE Transactions on Power Systems*, vol. 28, no. 3, pp. 3429–3439, Aug. 2013.

[15] J. E. Quiroz, M. J. Reno, O. Lavrova, and R. H. Byrne, "Communication requirements for hierarchical control of volt-var function for steady-state voltage," in *2017 IEEE Power Energy Society Innovative Smart Grid Technologies Conference (ISGT)*, Apr. 2017, pp. 1–5.

[16] F. Olivier, P. Aristidou, D. Ernst, and T. Van Cutsem, "Active Management of Low-Voltage Networks for Mitigating Overvoltages Due to Photovoltaic Units," *IEEE Transactions on Smart Grid*, vol. 7, no. 2, pp. 926–936, Mar. 2016.

[17] R. J. Broderick, J. E. Quiroz, M. J. Reno, A. Ellis, J. W. Smith, and R. C. Dugan, "Time Series Power Flow Analysis for Distribution Connected PV Generation," Sandia National Laboratories, Albuquerque, New Mexico, Tech. Rep. SAND2013-0537, Jan., 2013.

[18] R. Tonkoski, D. Turcotte, and T. H. El-Fouly, "Impact of high PV penetration on voltage profiles in residential neighborhoods," *IEEE Transactions on Sustainable Energy*, vol. 3, no. 3, pp. 518–527, Jul. 2012.

[19] IEEE Std 1547-2003, *IEEE Standard for Interconnecting Distributed Resources with Electric Power Systems*, 2003.

[20] R. Tonkoski and L. A. Lopes, "Impact of active power curtailment on overvoltage prevention and energy production of PV inverters connected to low voltage residential feeders," *Renewable Energy*, vol. 36, no. 12, pp. 3566–3574, Dec. 2011.

[21] D. P. Chassin, K. Schneider, and C. Gerkensmeyer, "GridLAB-D: An open-source power systems modeling and simulation environment," in *2008 IEEE/PES Transmission and Distribution Conference and Exposition*, Apr. 2008, pp. 1–5.

[22] T. M. Hansen, B. Palmintier, S. Suryanarayanan, A. A. Maciejewski, and H. J. Siegel, "Bus.py: A GridLAB-D communication interface for Smart distribution Grid simulations," in *2015 IEEE Power Energy Society General Meeting*, Jul. 2015, pp. 1–5.

[23] T. M. Hansen, E. K. P. Chong, S. Suryanarayanan, A. A. Maciejewski, and H. J. Siegel, "A Partially Observable Markov Decision Process Approach to Residential Home Energy Management," *IEEE Transactions on Smart Grid*, vol. 9, no. 2, pp. 1271–1281, Mar. 2018.

[24] PJM, *PJM estimated hourly load*. [Online]. Available: http://www.pjm.com/markets-and-operations/energy/real-time/loadhryr.aspx (visited on 03/05/2018).

[25] SolarAnywhere, *Clean Power Research*, 2017. [Online]. Available: https://www.solaranywhere.com (visited on 12/29/2017).

[26] SOLAR ELECTRIC SUPPLY, *8.4 KW SolarWorld Sunmodule Plus SW 280 Mono Solar Panel System*, 2017. [Online]. Available: https://www.solarelectricsupply.com/solarworld-8-4kw-sunmodule-plus-sw-280-mono-fronius-solar-system (visited on 12/20/2017).

[27] ComEd, *View a Sample Residential Bill*, 2018. [Online]. Available: https://www.comed.com/MyAccount/MyBillUsage/Pages/SampleResidentialBill2.aspx (visited on 03/14/2018).

[28] ComEd, *COMED'S HOURLY PRICING PROGRAM*, 2018. [Online]. Available: https://hourlypricing.comed.com/wp-content/uploads/2017/10/2017-HP-program-guide-v13.pdf (visited on 03/14/2018).

[29] ComEd, *ComEd residential real-time pricing program*, 2018. [Online]. Available: https://hourlypricing.comed.com/live-prices/ (visited on 03/18/2018).

[30] ComEd, *Rider TAX - Municipal and State Tax Additions*, 2018. [Online]. Available: https://www.comed.com/MyAccount/MyBillUsage/Pages/CurrentRatesTariffs.aspx (visited on 05/04/2018).

[31] S. J. Sheather and M. C. Jones, "A reliable data-based bandwidth selection method for kernel density estimation," *Journal of the Royal Statistical Society. Series B (Methodological)*, pp. 683–690, 1991.

[32] S. J. Sheather, "Density estimation," *Statistical science*, pp. 588–597, 2004.

[33] R. Fu, D. Feldman, R. Margolis, M. Woodhouse, K. Ardani, R. Fu, D. Feldman, R. Margolis, M. Woodhouse, and K. Ardani, "U . S . Solar Photovoltaic System Cost Benchmark : Q1 2017 U . S . Solar Photovoltaic System Cost Benchmark : Q1 2017," National Renewable Energy Laboratory, Tech. Rep., Sep. 2017.

[34] F. A. Felder and R. Athawale, "The life and death of the utility death spiral," *The Electricity Journal*, vol. 27, no. 6, pp. 9 –16, Jul. 2014.